Concept Design of a Scanning Laser Rangefinder for Autonomous Vehicles

Alonzo Kelly

CMU-RI-TR-94-21

The Robotics Institute
Carnegie Mellon University
5000 Forbes Avenue
Pittsburgh, PA 15213

January 24, 1995

This research was sponsored by ARPA under contracts “Perception for Outdoor Navigation” (contract number DACA76-89-C-0014, monitored by the US Army Topographic Engineering Center) and “Unmanned Ground Vehicle System” (contract number DAAE07-90-C-RO59, monitored by TACOM).

The views and conclusions expressed in this document are those of the author and should not be interpreted as representing the official policies, either express or implied, of the US government.

Abstract

This report specifies a scanning laser rangefinder which is specifically designed for high speed autonomous vehicles. This new scanner, called Tornado, represents a departure from conventional sensors in that it looks farther downrange in order to detect obstacles earlier. This made it possible to maintain a wide horizontal field of view, good obstacle resolving power, high throughput and good uniformity of the scan all at the same time. Tornado utilizes a narrow vertical field of view and a programmable vertical scan in order to achieve this.

While this report is not written to evaluate the performance limitations imposed by the current HMMWV configuration, it is clear from the analysis that the ERIM sensor is poorly suited to high speed off road navigation. For this reason, the Tornado scanner must be constructed in order to achieve 20 m.p.h. speeds.

A simple, general kinematic theory is presented which encompasses the kinematics transforms for all existing laser rangefinders. A short study of the design constraints that limit rangefinder performance is presented. The results of this work provide useful relationships for reference purposes.

Table of Contents

List of Figures

List of Symbols

f_{cells}	map cell throughput
f_{pixels}	sensor throughput, laser bandwidth
f_{images}	frame rate
f_{mirror}	mirror rpm
f_{cpu}	CPU speed
f_{comm}	communications bandwidth
h	sensor height
K_M	mirror gain
R	range
T_{images}	frame period
V	vehicle speed
x	crossrange coordinate
y	downrange coordinate
z	vertical coordinate
δ	map resolution
η_S	scanning efficiency
η_T	laser duty cycle
η_G	geometric efficiency
ψ	beam azimuth angle
σ	area density
σ_I	imaging density
σ_S	scanning density
θ	beam elevation angle
$\dot{\theta}$	vertical sweep rate
Ψ	sensor flux
β	sensor tilt angle
ω	angular velocity

1. Introduction

At the speeds required of the next generation of autonomous vehicles, it becomes necessary to explicitly address the need for the vehicle to react to hazards in real time. As speeds increase, computing and sensory hardware must be re-evaluated to remove the bottlenecks that were acceptable at the lower speeds encountered in earlier research.

Higher speeds require both looking further ahead and reacting faster. Hence, autonomous navigation must mature to the point where significantly more computation is performed in less time. While computing engines continue to increase in capability, off road sensory systems have improved little for a decade.

This report outlines a concept design for a scanning laser rangefinder, called the Tornado, which is customized to support high speed off road navigation of the HMMWV. The design is based on the analysis presented in [5].

1.1 Acknowledgments

Dan Christian, Barry Brumitt, R. Coulter, Tony Stentz, Martial Hebert, Chuck Thorpe, and Dean Pomerleau have contributed important ideas to this report. The section on scanning mechanisms could not have been written without Dan Christian's help. The impetus for this work was the realization that CMU could actually construct its own rangefinder - as was done by Brian Smith on the Erebus program.

1.2 Analytical Basis of the Concept

A few aspects of the analysis presented in [5] are central to the design of the sensor. These will be briefly reviewed here.

1.2.1 Geometric Efficiency

The **geometric efficiency** of a sensor is defined as the inverse of the average number of times that the same small patch of terrain is measured. This quantity has two components. The **scanning density** is the average number of pixels from the same image that fall on the patch. The **imaging density** is the average number of images that fall on the patch.

1.2.2 Adaptive Sweep

The primary reason for poor geometric efficiency of sensors is the wide vertical field of view necessary to ensure coverage on rough terrain. However, the dynamic requirements on the vertical field of view that ensure coverage can be two orders of magnitude less. **Adaptive sweep** is the principle of modulating the vertical width of the field of view in order to guarantee coverage of the environment while maintaining a reasonable imaging density.

1.2.3 Adaptive Scan

A second reason for poor geometric efficiency is the typical 10:1 aspect ratio of pixels on the ground. The principle of **adaptive scan** is to elongate pixels in the reverse direction in image space in order to ensure roughly square pixel resolution on the groundplane.

2. Physical and Interface Requirements

This section states some requirements associated with the physical mechanisms, mass properties, and computer interfaces to the sensor.

2.1 Ease of Calibration

For the purposes of easy calibration, it would be useful to include a visible laser which is coaxial with the IR ranging laser. Further, sensor drive electronics should support a control mode which shuts off the continuous scan and drives the beam to a designated angular position. In this way, the cartesian position of the visible laser spot can be correlated with the beam angles.

The alignment of the laser beam with the mirrors is critical to the accuracy of the sensor kinematic transforms. For this reason, alignment screws should be provided which permit aligning the input beam with the sensor housing.

2.2 Eye Safety

Laser parameters are to be chosen to ensure eye safety. However, sensor signal to noise characteristics are, of course, worsened by low power levels, so it important not to overly limit the laser power level.

2.3 Environmental Protection

The entire sensor mechanism is to be enclosed in a water proof enclosure to protect the electronics and sensitive optics from water damage. A Nitrogen port and desiccant indicator should be considered to maintain a moisture and dust free internal atmosphere.

2.4 Ease of Installation

The sensor will be used on a prototype autonomous vehicle which serves as a testbed for diverse research projects. As a result, ease of installation and removal, permitting rapid changeout of the sensor with other sensing devices, is a primary concern.

A simple mounting bracket is required which is also mechanically repeatable. The bracket must maintain repeatability of the three axis orientation of the sensor with respect the vehicle to within 1/10 of a degree.

As far as is possible, the system should weigh less than 20 lbs or be composed of modules less than 20 lbs in weight. This is to permit installation by a single person.

2.5 Run-Time Programmability

In order to support ease of reconfiguration of scanning parameters and to support real time sensor pointing, an interface command language should be supported by the sensor to permit application control of the scanning pattern in real time. As a minimum requirement, the vertical field of view must be configurable in both angular width and position relative to the horizon. That is, both the highest and lowest scanline must be independently programmable.

2.6 Reflectance Channel

The sensor should provide a reflectance channel in order to support a more diverse research agenda.

2.7 Integral Computing

The highest computational load required in autonomous navigation is the geometric processing of the range image (ignoring the load of generating it for stereo). Therefore, special purpose high speed hardware should be considered to mechanize the transform equations in real time.

2.8 Integral Position Estimation

Perception requires higher frequency position updates than does vehicle motion control. Therefore, the sensor should be configured to include integral high speed position estimation or, at least, there must be a high bandwidth link between the sensor and position estimation. Bandwidth, must be sufficient to sample the vehicle attitude at five to ten times the Nyquist rate.

3. Accuracy and Resolution Requirements

Perhaps the most important requirement on a rangefinder is its ability to detect, localize, and resolve obstacles. This section considers the matter of mapping the size of an obstacle which is to be detected onto the required linear and angular resolution of the sensor.

3.1 Differential Resolution Relationships

The **instantaneous field of view** is the angular width of the laser beam[1]. This is also known as the **beam dispersion**. The angular coordinates of the beam are often expressed in terms of horizontal sweep or **azimuth** ψ, and vertical sweep or **elevation** θ. When elevation is measured down from the horizon, it is called **depression**. The relationships between the beam width and its projections onto three orthogonal axes are given below. In the analysis, three orthogonal axes are considered to be oriented along the vehicle body axes of symmetry:

- x - **crossrange**, in the groundplane, normal to the direction of travel
- y - **downrange**, in the groundplane, along the direction of travel
- z - **vertical**, normal to the groundplane

Note that the differential relationships come from projective geometry and not from differentiating the coordinate transforms. More precise relationships are available from the Jacobian of the coordinate transformation, but this depends on the precise scanning pattern chosen. In order to avoid dependence on the scanning pattern, the following approximations are used which are good enough for the purpose of the discussion here:

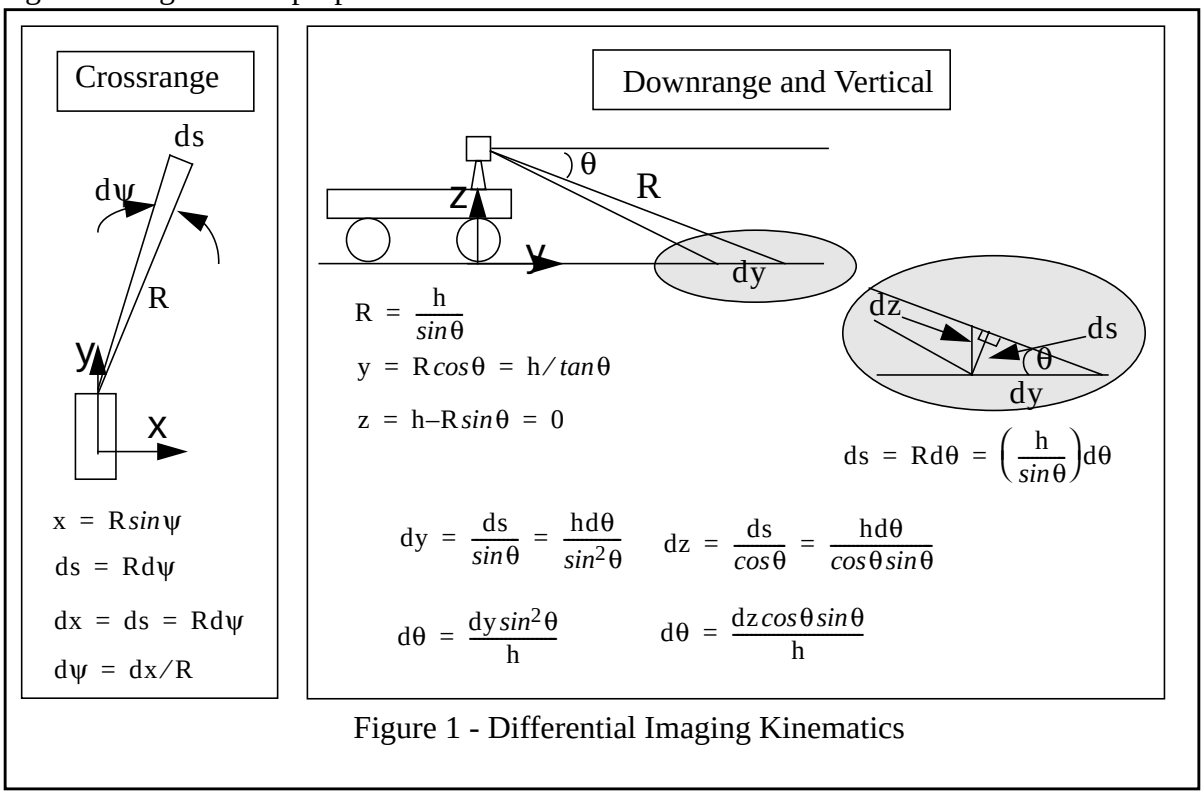

Figure 1 - Differential Imaging Kinematics

1. Actually, the IFOV is the angle subtended by the **receive** optics, but this distinction will be ignored here.

3.2 Forward Resolution Transforms

The relationships which give the cartesian differentials dx, dy, and dz in terms of the IFOV, will be called the **forward resolution transforms**. The following graphs give the cartesian differentials versus range for various values of the IFOV. In each, the extent of the abscissa is from the y coordinate at -30 degrees at the low end to 50 meters at the high end. Clearly the crossrange and vertical relationships are well approximated by the linear law for small angles, ***the downrange sampling however, is dominated by the projection onto the groundplane***.

These relationships can be used to read both the spot size of the laser beam as a function of the IFOV at any range as well as the spacing between spots as a function of the angular deviation of scanning mirrors at any range. Notice that at high ranges, downrange spot size and spacing is 20 times what it is in the other two directions.

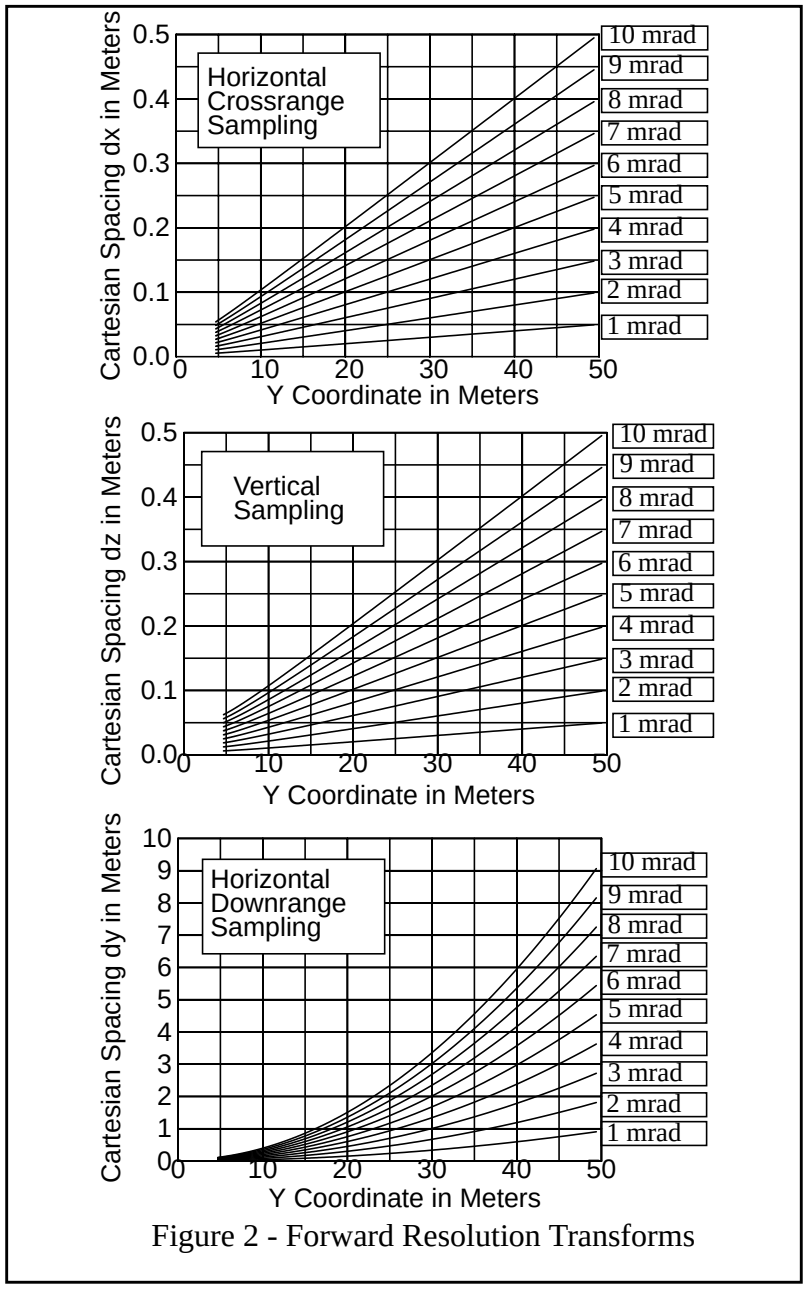

Figure 2 - Forward Resolution Transforms

3.3 Inverse Resolution Transforms

The relationships which give the IFOV in terms of the cartesian differentials are called the **inverse resolution transforms**. The following graphs give the polar differentials versus range for various values of the cartesian differentials. In each, the extent of the abscissa is from the y coordinate at -30 degrees at the low end to 50 meters at the high end.

These relationships can be used to read the required spot size of the laser beam as well as the required angular spacing of range pixels in order to give a particular cartesian spacing along any of the three axes.

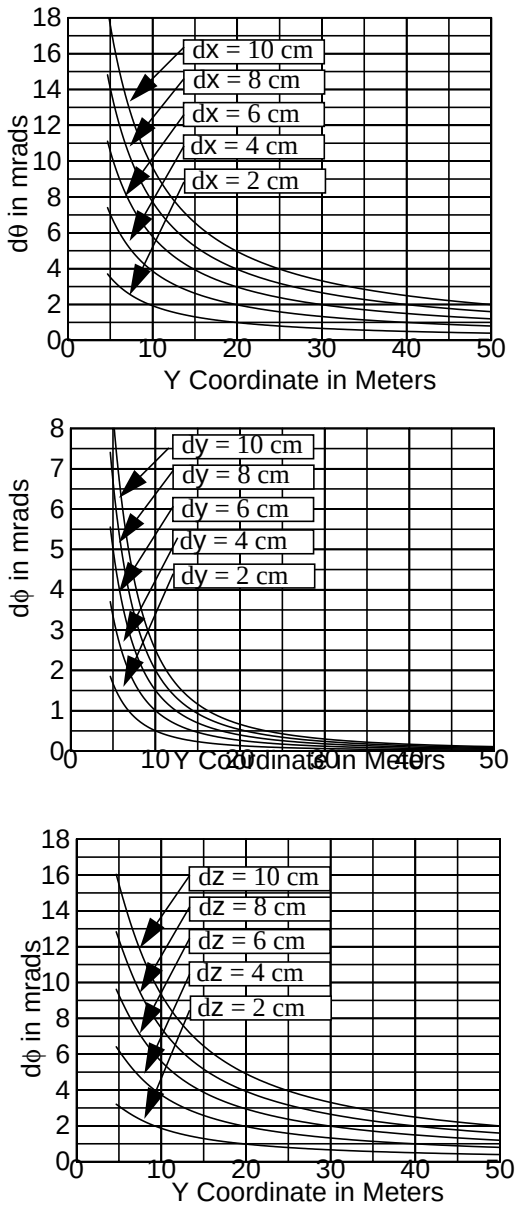

Figure 3 - Inverse Resolution Transforms

3.4 Rate Relationships

The inverse resolution transforms also give the rotational rates required of the beam, and hence of the scanning mirrors, in order to give a particular velocity of the spot on the groundplane:

$$\frac{d\theta}{dt} = \left(\frac{sin^2\theta}{h}\right)\frac{dy}{dt} \qquad \text{and} \qquad \frac{d\psi}{dt} = \left(\frac{1}{R}\right)\frac{dx}{dt}$$

3.5 Angular Accuracy

In order to ensure that the position of the laser footprint is known to within the resolution of the map, it is necessary that the angular position of the beam be known and repeatable to an accuracy equal to the IFOV. The worst case IFOV from the previous graphs at 50 meter range is 0.1 mrads. Constant systematic error is acceptable but adjacent pixels must be known and repeatable to 0.1 mrads.

3.6 Range Accuracy

In order to ensure that the position of the laser footprint is known to within the resolution of the map, it is necessary that the range reading be accurate to a size on the order of the map cell size. Assuming a cell size of 1/6 meter, an accuracy of about 2 cm is necessary. Systematic range error is acceptable, but ***relative range accuracy*** across an entire image should exceed 2 cm.

4. Scanning Pattern Requirements

This section considers the scanning pattern of the sensor.

4.1 Scanning Kinematics

Two degrees of freedom - azimuth and elevation - are required to scan the environment in 2-1/2 D. There are two possible ways to do this kinematically because either the azimuth rotation or the elevation rotation can come first. This statement assumes that the two degrees of freedom are orthogonal, because it simplifies the computations required in the perception system. Note that this issue is independent of the physical scanning of the beam. At issue here is the order in which the beam experiences the necessary rotations. The physical scan depends on the relative rates of the scanning mirrors. The scan footprints of the two possibilities are indicated below:

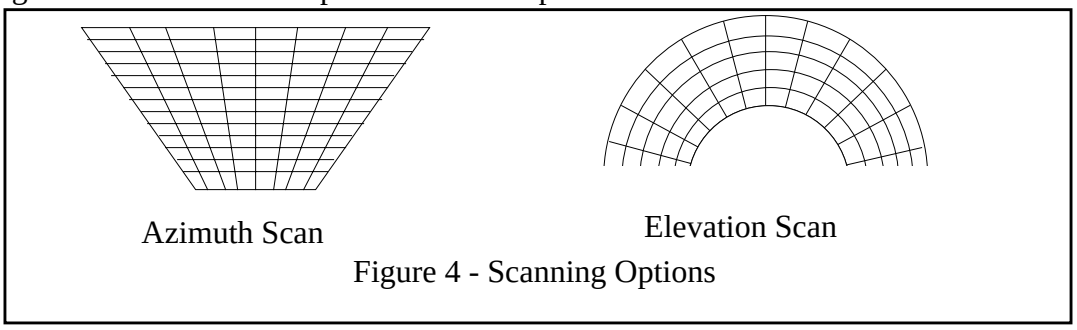

Figure 4 - Scanning Options

The two alternatives differ in whether lines of constant elevation or of azimuth are straight on flat terrain. The elevation scan has a regular increase of density with elevation, independent of azimuth. The lines of constant azimuth in the azimuth scan are really hyperbolas, so the elevation scan is preferred from the point of view of calculating downrange step discontinuities. This is particularly true in wide horizontal field of view sensors. The preference of one pattern over another depends mostly on how closely the vehicle approximates omnidirectionality at the maximum sensor range.

4.2 Scan Order

The order of the scan specifies which degree of freedom cycles faster than the other. It is most consistent with path planning algorithms with a planning horizon to consider that geometry is known to equal distance in all directions at any given time. Hence, the azimuth degree of freedom must cycle faster than the elevation based on this consideration.

However, from the point of view of computing accurate downrange step discontinuities, the vehicle motion between two pixels that are adjacent in the same column is far more than in the opposite case leading to less accuracy in detecting small obstacles. This consideration leads to the opposite conclusion. The preference of one alternative over the other depends heavily on the frame rate and the relative contribution of range error, beam dispersion, and vehicle position error to the error in terrain slope computations.

4.3 Scan Direction

The sensor maximum range is decreased by the motion of the vehicle, so it is most effective to scan from bottom to top in elevation. For a fixed angular resolution sensor, vertical pixel overlap should be tuned to the design velocity. On average, scanning from top to bottom does not ensure that obstacles are seen as early as possible, as it may seem at first glance that it does. The direction of the azimuth scan is immaterial.

5. Optical Kinematics

The kinematics of reflecting a laser beam from a mirror are central to the operation of the current generation of laser rangefinders. This section will outline a general technique for modelling such rangefinders.

5.1 The Reflection Operator

From Snell's law for reflection of a ray:

- the incident ray, the normal to the surface, and the reflected ray, all lie in the same plane.
- the angle of incidence equals the angle of reflection

From these two rules, a very useful matrix operator can be formulated to reflect a vector off of any surface, given the unit normal to the surface. Consider a vector $\vec{v}_i$, not necessarily a unit vector, which impinges on a reflecting surface at a point where the unit normal to the surface is $\hat{n}$. Unless they are parallel, the incident and normal vector define a plane, which will be called the **reflection plane**. Drawing both vectors in this plane, it is clear that Snell's law can be written in many forms:

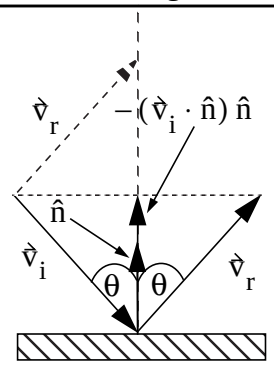

$$\vec{v}_r = \vec{v}_i - 2\,(\vec{v}_i \cdot \hat{n})\,\hat{n}$$

$$\vec{v}_r = \vec{v}_i - 2v_i \cos\theta\,\hat{n}$$

$$\vec{v}_r = \vec{v}_i - 2\,(\hat{n} \otimes \hat{n})\,\vec{v}_i$$

$$\vec{v}_r = \mathrm{Ref}\,(\hat{n})\,\vec{v}_i$$

$$\mathrm{Ref}\,(\hat{n}) = I - 2\,(\hat{n} \otimes \hat{n})$$

$$\mathrm{Ref}\,(\hat{n}) = \begin{bmatrix} 1-2n_xn_x & -2n_xn_y & -2n_xn_z \\ -2n_yn_x & 1-2n_yn_y & -2n_yn_z \\ -2n_zn_x & -2n_zn_y & 1-2n_zn_z \end{bmatrix}$$

Where the outer product ($\otimes$) of the normal with itself was used in forming the matrix equivalent.

The result is expressed in the same coordinates in which both the normal and the incident ray were expressed. This can be used to model the "optical" kinematics of laser rangefinders. Notice that a reflection is equivalent to a rotation of twice the angle of incidence about the normal to the reflection plane A similar matrix refraction operator can be defined.

In order to model rangefinders, the laser beam will be modelled by a unit vector since the length of the beam is immaterial. The unit vector is operated upon by the reflection operator - one reflection for each mirror. The ultimate result of all reflections will be expressed in the original coordinate system.

The basic idea is that, since the mirrors are flat, the reorientation of the beam is independent of exactly where it hits the mirror. This is justified because Snell's law states that the direction of any reflected beam depends only on the direction of the normal to any mirror and the direction of the incident beam.

The results of such an analysis give the orientation of the laser beam as a function of the actuated mirror angles, but it says nothing about where the beam is positioned in space. The precise position of the beam is not difficult to calculate and is important in the sizing of mirrors. From the point of view of computing kinematics, beam position is irrelevant, so it will be ignored here.

5.2 The Vector Projection Operator

The projection of one vector onto another is trivially given by the dot product. Consider a vector $\vec{v}_i$, not necessarily a unit vector, which is to be projected onto a unit vector $\hat{n}$. The projection rule can be written in many forms:

$$\vec{v}_p = (\vec{v}_i \cdot \hat{u})\,\hat{u}$$

$$\vec{v}_p = v_i \cos\theta\,\hat{u}$$

$$\vec{v}_p = \text{Projv}(\hat{u})\,v_i$$

$$\text{Projv}(\hat{n}) = \hat{n} \otimes \hat{n}$$

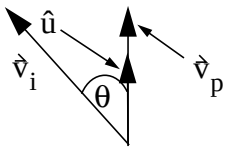

$$\text{Projv}(\hat{n}) = \begin{bmatrix} n_x n_x & n_x n_y & n_x n_z \\ n_y n_x & n_y n_y & n_y n_z \\ n_z n_x & n_z n_y & n_z n_z \end{bmatrix}$$

5.3 The Plane Projection Operator

The projection of a vector into a plane is a simple matter. The basic operation is to remove the component of the vector along the normal to the plane. Consider a vector $\vec{v}_i$, not necessarily a unit vector, which is to be projected on a surface at a point where the unit normal to the surface is $\hat{n}$. This plane will be called the **projection plane**. The operator can be written in many ways:

$$\vec{v}_p = \vec{v}_i - (\vec{v}_i \cdot \hat{n})\,\hat{n}$$

$$\vec{v}_p = \vec{v}_i - v_i \cos\theta\,\hat{n}$$

$$\vec{v}_p = \hat{n} \times (\hat{n} \times \vec{v}_i)$$

$$\vec{v}_p = \text{Projp}(\hat{n})\,\vec{v}_i$$

$$\text{Projp}(\hat{n}) = I - (\hat{n} \otimes \hat{n})$$

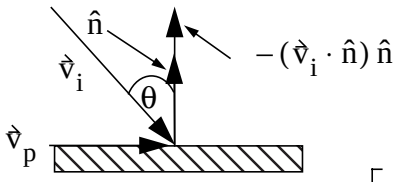

$$\text{Projp}(\hat{n}) = \begin{bmatrix} 1 - n_x n_x & -n_x n_y & -n_x n_z \\ -n_y n_x & 1 - n_y n_y & -n_y n_z \\ -n_z n_x & -n_z n_y & 1 - n_z n_z \end{bmatrix}$$

The expression involving the vector cross product was generated by noting that $\vec{v}_p$ is oriented along the vector $\hat{n} \times (\hat{n} \times \vec{v}_i)$ and has magnitude $v_i \sin\theta$. The result is expressed in the same coordinates in which both the normal and the incident ray were expressed. It is useful for determining the kinematics of parallel laser beams when they are transformed by the scanning mechanism.

5.4 Rate Relationships

Consider now the problem of predicting the angular velocity of the reflected ray when the incident ray is reflected off a mirror that is rotating. This is, after all, exactly how a scanning mechanism works. Let the mirror rotate about a general axis in space. Its angular velocity is denoted by $\vec{\omega}_n$. This rotation of the mirror gives rise to a rotation $\vec{\omega}_r$ of the reflected beam. In the completely general case, the incident beam may rotate as well with velocity $\vec{\omega}_i$. However, since it is clear that the angular velocity of the normal with respect to the incident beam is the quantity that matters, $\hat{v}_i$ can be considered to be fixed with the understanding that its angular velocity must be added to that of the normal when it is not fixed.

This problem can be solved using concepts of moving reference frames. Consider an observer fixed in the reflection plane. The observer is not fixed in the frame of the mirror because the reflection plane may rotate about the mirror normal. Let the angular velocity of the moving observer in the frame fixed to the sensor housing be $\vec{\omega}$. Angular velocities are true vectors which add in the usual way. Hence, the angular velocity of the output beam in the fixed frame is just the sum of what the moving observer sees and the motion of the moving observer:

$$\vec{\omega}_r = \vec{\omega}_r\Big|_{moving} + \vec{\omega}$$

Lets establish a coordinate system fixed to the projection plane consisting of the mirror normal $\hat{n}$, the normal to the projection plane $\hat{o}$, and the cross product of these two $\hat{a}$. This system is shown in the following figure:

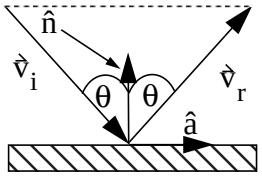

$$\hat{o} = \frac{(\hat{v}_i \times \hat{n})}{\left|(\hat{v}_i \times \hat{n})\right|}$$

NOTE: $\hat{o}$ points out of the paper

$$\hat{a} = (\hat{n} \times \hat{o})$$

Now, from the point of the moving observer, the motion of the reflected beam is given by the rate of change of θ and, as a vector, it is directed normal to the reflection plane:

$$\vec{\omega}_r\Big|_{moving} = \dot{\theta}\hat{o}$$

Note there is no factor of two in the moving frame since the mirror normal vector is fixed in the moving frame. Now $\dot{\theta}$ is the projection of the angular velocity of $\vec{\omega}_n$ onto the normal to the reflection plane:

$$\vec{\omega}_r\Big|_{moving} = [\vec{\omega}_n \cdot \hat{o}]\,\hat{o}$$

The angular velocity of the reflection plane is equal to that of the mirror minus the component which is oriented along the mirror normal, since rotation around the mirror normal does not rotate the projection plane. This is, of course, the projection into the plane of the mirror itself:

$$\vec{\omega} = \vec{\omega}_n - (\vec{\omega}_n \cdot \hat{n})\,\hat{n}$$

Hence, the complete result is:

$$\vec{\omega}_r = [\vec{\omega}_n \cdot \hat{o}]\,\hat{o} + \vec{\omega}_n - (\vec{\omega}_n \cdot \hat{n})\,\hat{n}$$

This result is intuitively correct because it contains two times the $\hat{o}$ component of $\vec{\omega}_n$, one times the $\hat{a}$ component of $\vec{\omega}_n$, and zero times the $\hat{n}$ component of $\vec{\omega}_n$. This can be written in terms of the operators given so far as follows:

$$\vec{\omega}_r = [2\,\mathrm{Projv}(\hat{o}) + \mathrm{Projv}(\hat{a})]\,\vec{\omega}_n$$

In words, ***the angular velocity of the reflected beam is twice the projection of the mirror angular velocity onto the reflection plane normal plus the projection onto the axis normal to both the reflection plane normal and the mirror normal***[2].

5.5 Mirror Gain

Define the **mirror gain** K_M in terms of the angular velocity of the beam ω_r and the angular velocity of the mirror ω_n as follows:

$$K_M = \frac{\omega_r}{\omega_n}$$

The mirror gain can vary from 0 to 2 depending on the orientation of the input beam, the mirror normal, and the mirror angular velocity. The above result explains why the beam enters the polygonal mirror from the side in the ERIM scanner - because there is a gain of 2 in only that direction. In the Hurricane scanner, the beam enters along $\hat{a}$ axis, so the gain is 1. Note also, that a two axis scanner requires two separate mirrors in order to get a gain of 2 in both axes.

This gain can be a very significant factor in the design of a rangefinder since the angular velocity of mirrors is a major limiting factor. ***Throughput can be doubled by appropriate scanning mechanism design.***

2. See Optics by Hecht for a verification of this surprising result.

5.6 Composition of Translation and Reflection

Consider now the issues involved with using two parallel laser transmitters. Peculiar things can happen when two parallel beams enter a system of mirrors. In the ERIM scanner for instance, if two beams enter the mirrors spaced along the z axis, they leave spaced along the x axis, if they enter spaced along the y axis, they leave spaced along the z axis, and finally if they enter spaced along the x axis, they are coincident, and can be considered to leave spaced along the y axis.

This behavior is explained in the following figure. Consider two parallel incident beams $\vec{v}_{1i}$ and $\vec{v}_{2i}$ which are separated by a perpendicular translation vector $\vec{t}_i$. The perpendicular translation is used since beams are themselves lines and otherwise have no unique relative translation.

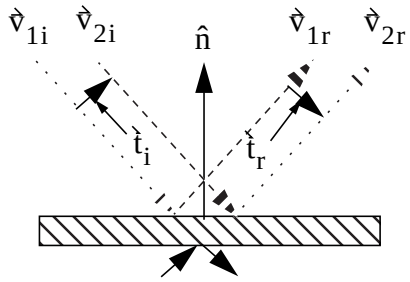

$$\vec{v}_{1r} = \vec{v}_{1i} - 2\,(\vec{v}_{1i} \cdot \hat{n})\,\hat{n}$$

$$\vec{v}_{2i} = \text{Trans}\,(\vec{t}_i)\,\vec{v}_{1i} = \vec{t}_i + \vec{v}_{1i}$$

$$\vec{v}_{2r} = \text{Ref}\,(\hat{n})\,\vec{v}_{2i}$$

$$\vec{v}_{2r} = \text{Ref}\,(\hat{n})\,\text{Trans}\,(\vec{t}_i)\,\vec{v}_{1i}$$

$$\vec{v}_{2r} = \left(\vec{t}_i + \vec{v}_{1i}\right) - 2\left[\left(\vec{t}_i + \vec{v}_{1i}\right) \cdot \hat{n}\right]\hat{n}$$

$$\vec{v}_{2r} = \left(\vec{t}_i + \vec{v}_{1i}\right) - 2\left[\vec{t}_i \cdot \hat{n} + \vec{v}_{1i} \cdot \hat{n}\right]\hat{n}$$

$$\vec{v}_{2r} = \left(\vec{t}_i + \vec{v}_{1i}\right) - 2\,[\vec{t}_i \cdot \hat{n}]\,\hat{n} - 2\,[\vec{v}_{1i} \cdot \hat{n}]\,\hat{n}$$

$$\vec{v}_{2r} = \vec{t}_i - 2\,[\vec{t}_i \cdot \hat{n}]\,\hat{n} + \vec{v}_{1i} - 2\,[\vec{v}_{1i} \cdot \hat{n}]\,\hat{n}$$

$$\boxed{\vec{v}_{2r} = \text{Ref}\,(\hat{n})\,\vec{t}_i + \vec{v}_{1r}}$$

Many conclusions can be drawn from this result:

- The translation vector itself is reflected as if it was a beam entering through the back of the mirror.
- Since the reflection operator preserves the length of the incident vector, the relative perpendicular translation of the two beams is preserved as well. Note however that while the ***perpendicular*** distance is preserved, the ***projection*** of the distance between the two beams onto any surface changes.
- If a component of the translation vector exists out of the reflection plane, it is left unchanged, so the above expression is completely general.
- As a convenient mnemonic, whenever the translation vector has a component along the mirror normal, that component is flipped by the reflection operation, and the two beams switch places along the normal direction.

5.7 Composition of Rotation and Reflection

A basic property of plane mirrors is the formation of an image ***behind*** the mirror. This property arises from the conservation of the relative angles between rays emanating from a point source. This behavior is explained in the following figure. Consider two incident beams $\hat{v}_{1i}$ and $\hat{v}_{2i}$ which are separated by an angle θ. Since both beams are unit vectors, their dot product is a direct measure of the angle between them.

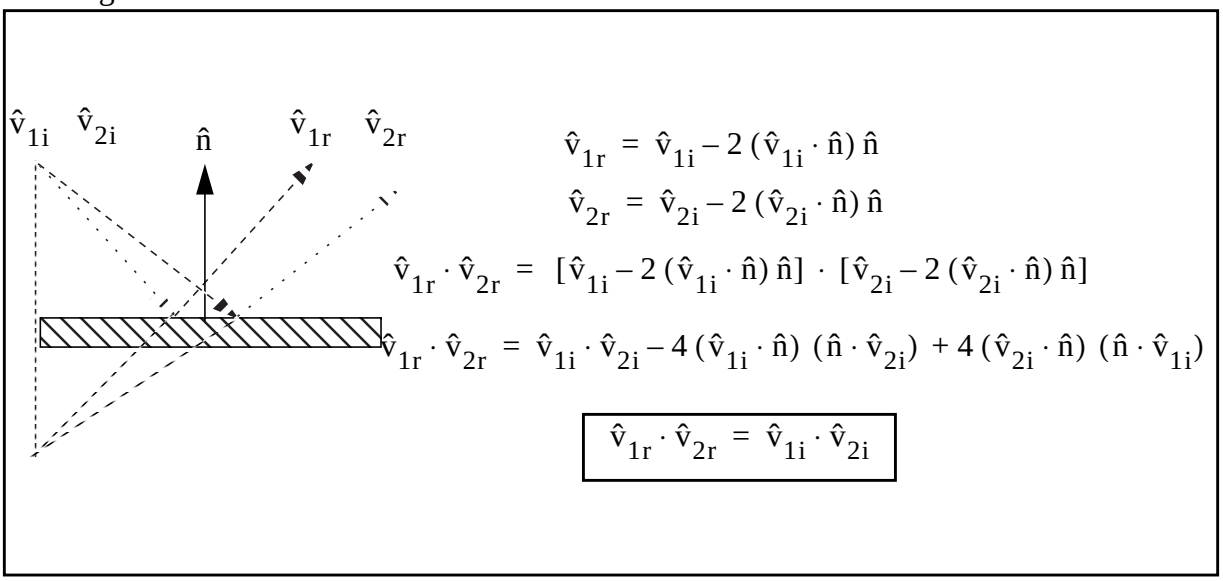

$$\hat{v}_{1r} = \hat{v}_{1i} - 2\,(\hat{v}_{1i} \cdot \hat{n})\,\hat{n}$$

$$\hat{v}_{2r} = \hat{v}_{2i} - 2\,(\hat{v}_{2i} \cdot \hat{n})\,\hat{n}$$

$$\hat{v}_{1r} \cdot \hat{v}_{2r} = [\hat{v}_{1i} - 2\,(\hat{v}_{1i} \cdot \hat{n})\,\hat{n}] \cdot [\hat{v}_{2i} - 2\,(\hat{v}_{2i} \cdot \hat{n})\,\hat{n}]$$

$$\hat{v}_{1r} \cdot \hat{v}_{2r} = \hat{v}_{1i} \cdot \hat{v}_{2i} - 4\,(\hat{v}_{1i} \cdot \hat{n})\,(\hat{n} \cdot \hat{v}_{2i}) + 4\,(\hat{v}_{2i} \cdot \hat{n})\,(\hat{n} \cdot \hat{v}_{1i})$$

$$\boxed{\hat{v}_{1r} \cdot \hat{v}_{2r} = \hat{v}_{1i} \cdot \hat{v}_{2i}}$$

Thus the angle between the reflected beams is equal to the angle between the incident beams. This means that a point source reflected by a mirror forms an image behind the mirror. The laser transmitter of a rangefinder can be modelled as a point source. The implication is that ***the projection of the laser spot on the groundplane is just the intersection of a cone surrounding the beam and the groundplane.***

5.8 Intersection of a Line and a Plane

The intersection of a line and a plane is the basis for a complete ray tracing simulation of the internal kinematics of rangefinders. This permits computation of the precise spot pattern of the rangefinder, and the required size of the mirrors. Let a line be defined by a vector $\hat{v}$ to which it is parallel and a point $\hat{r}_L$ which lies on the line. Let a plane be defined by a vector $\hat{n}$ normal to the plane and a point $\hat{r}_P$ which lies on the plane. The general solution to the problem is given in the following figure by a matrix equation.

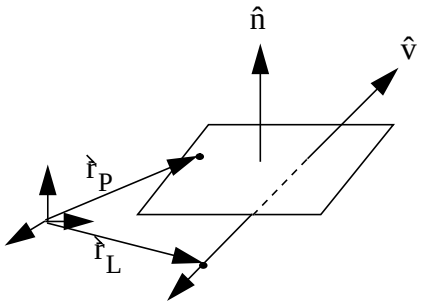

Plane: $n_x (x - x_p) + n_y (y - y_p) + n_z (z - z_p) = 0$

Line: $\dfrac{x - x_L}{v_x} = \dfrac{y - y_L}{v_y} = \dfrac{z - z_L}{v_z}$

$$n_x x + n_y y + n_z z = n_x x_p + n_y y_p + n_z z_p$$

$$v_y x - v_x y = v_y x_L - v_x y_L$$

$$v_z y - v_y z = v_z y_L - v_y z_L$$

$$\begin{bmatrix} n_x & n_y & n_z \\ v_y & -v_x & 0 \\ 0 & v_z & -v_y \end{bmatrix} \begin{bmatrix} x \\ y \\ z \end{bmatrix} = \begin{bmatrix} \hat{n} \cdot \hat{r}_P \\ v_y x_L - v_x y_L \\ v_z y_L - v_y z_L \end{bmatrix}$$

6. Kinematics of the Azimuth Scanner

The **azimuth scanner** is a generic name for a class of laser rangefinders with equivalent kinematics. In this scanner, the laser beam undergoes the azimuth rotation/reflection first and the elevation rotation/reflection second. Both the ERIM scanner and the Perceptron fall into this category. Both scanners are 2D scanning laser rangefinders employing a “polygonal” azimuth mirror and a flat “nodding” elevation mirror. The mirrors move as shown below:

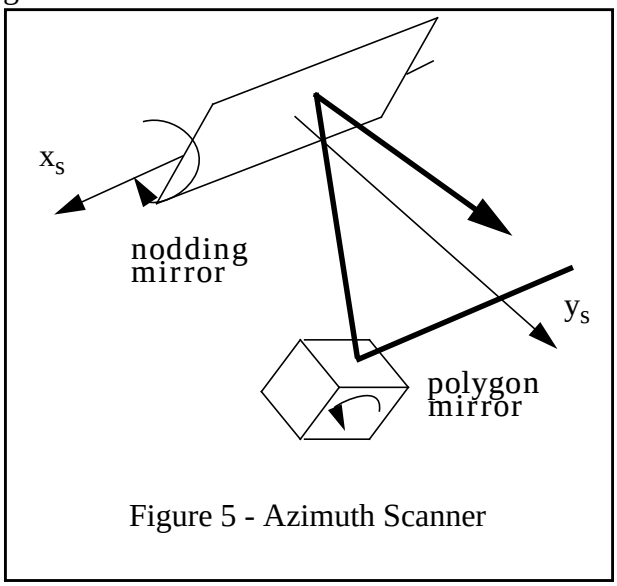

Figure 5 - Azimuth Scanner

A coordinate system called the “s” system is fixed to the sensor with y pointing out the front of the sensor and x pointing out the right side. The beam enters along the x_s axis. It reflects off the polygonal mirror which rotates about the y_s axis. It then reflects off the nodding mirror, to leave the housing roughly aligned with the y_s axis.

First, the beam is reflected from the laser diode about the normal to the polygonal mirror. Computation of the output of the polygonal mirror can be done by inspection by noting that the beam rotates by twice the angle of the mirror because it is a reflection operation, and the z-x plane contains both the incident and normal vectors. The datum position of the mirror should correspond to a perfectly vertical beam, so the datum for the mirror rotation angle is chosen appropriately.

Consider an input beam $\hat{v}_m$ along the x_s axis and reflect it about the mirror by inspection:

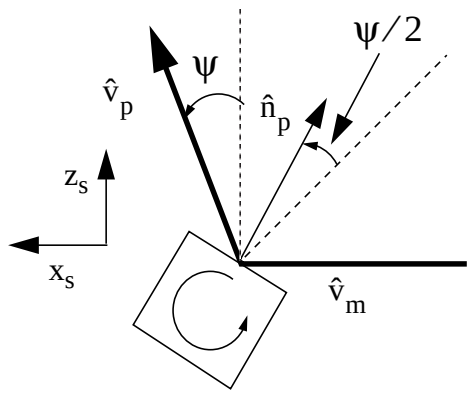

$$\hat{v}_m = \begin{bmatrix} 1 & 0 & 0 \end{bmatrix}^T$$

$$\hat{v}_p = \mathrm{Ref}(\hat{n}_p)\,\hat{v}_m$$

$$\hat{v}_p = \begin{bmatrix} s\psi & 0 & c\psi \end{bmatrix}^T$$

Figure 6 - Polygonal Reflection

Notice that this vector is contained within the x_s-z_s plane. Now this result must be reflected about the nodding mirror. Notice that, at this point, $\hat{v}_p$ cannot be simply rotated around the x axis since the axis of rotation which is equivalent to a reflection is normal to both $\hat{v}_p$ and $\hat{n}_n$. Since $\hat{v}_p$ is not always in the y_s-z_s plane, the x_s axis is not always the axis of rotation.

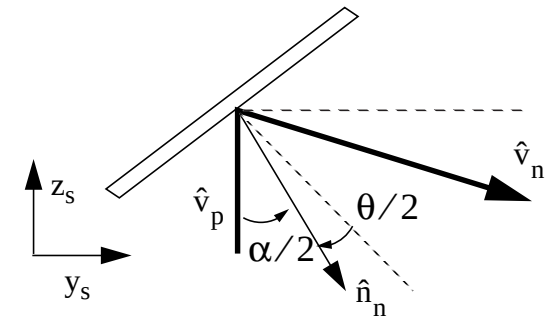

$$\hat{v}_p = \begin{bmatrix} s\psi & 0 & c\psi \end{bmatrix}^T$$

$$\text{put} \quad \frac{\alpha}{2} = \frac{\pi}{4} - \frac{\theta}{2}$$

$$\hat{n}_n = \begin{bmatrix} 0 & s\frac{\alpha}{2} & -c\frac{\alpha}{2} \end{bmatrix}^T$$

$$\hat{v}_n = \mathrm{Ref}(\hat{n}_n)\,\hat{v}_p = \hat{v}_p - 2(\hat{v}_p \cdot \hat{n}_n)\,\hat{n}_n$$

$$\hat{v}_n = \begin{bmatrix} s\psi \\ 0 \\ c\psi \end{bmatrix} + 2c\psi c\frac{\alpha}{2}\begin{bmatrix} 0 \\ s\frac{\alpha}{2} \\ -c\frac{\alpha}{2} \end{bmatrix} = \begin{bmatrix} s\psi \\ c\psi s\alpha \\ -c\psi c\alpha \end{bmatrix} = \begin{bmatrix} s\psi \\ c\psi s\left(\frac{\pi}{2} - \theta\right) \\ -c\psi c\left(\frac{\pi}{2} - \theta\right) \end{bmatrix}$$

$$\hat{v}_n = \begin{bmatrix} [s\psi] & [c\psi c\theta] & -[c\psi s\theta] \end{bmatrix}^T$$

Figure 7 - Nodding Reflection

Which is the required result. This result is summarized in the following figure:

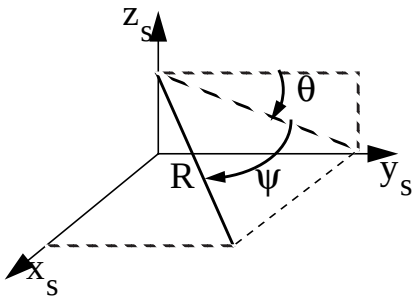

$$x_s = Rs\psi$$
$$y_s = Rc\theta c\psi$$
$$z_s = -Rs\theta c\psi$$

Figure 8 - Azimuth Kinematics

Thus, the kinematics of the azimuth scanner are equivalent to a rotation around the x_s axis followed by a rotation around the ***new*** z_s axis. By a theorem of 3D rotations, this is also equivalent to two rotations in the opposite order about fixed axes.

6.1 The Analytic Range Image of Flat Terrain

Given the basic kinematic transform, many analyses can be performed. The first is to compute an analytic expression for the range image of a perfectly flat piece of terrain. Let the sensor fixed "s"

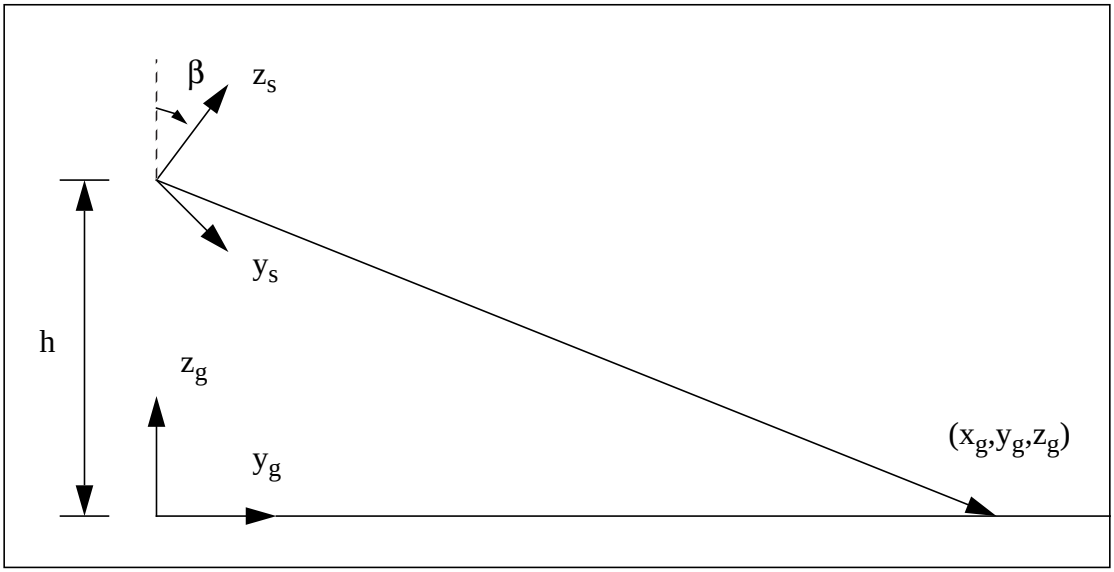

coordinate system be mounted at a height h and tilted forward by a tilt angle of β. Then, the transform from sensor coordinates to global coordinates is:

$$x_g = x_s$$
$$y_g = y_s c\beta + z_s s\beta$$
$$z_g = -y_s s\beta + z_s c\beta + h$$

If the kinematics are substituted into this, the transform from the polar sensor coordinates to global

coordinates is obtained:

$$x_g = R s\psi$$
$$y_g = (R c\theta c\psi)\, c\beta - (R s\theta c\psi)\, s\beta = R c\theta\beta c\psi$$
$$z_g = (-R c\theta c\psi)\, s\beta - (R s\theta c\psi)\, c\beta + h = h - R s\theta\beta c\psi$$

Now by setting $z_g = 0$ and solving for R, the expression for R as a function of the beam angles ψ and θ for flat terrain is obtained. This is an analytic expression for the range image of flat terrain under the azimuth transform.

$$R = h / (c\psi s\theta\beta)$$

Notice that when R is large $s\theta\beta = h/R$. This is the perception ratio defined earlier. As a check on the range image formula, the resulting range image is shown below for $h = 2.7$, $\beta = 16.5°$, a HFOV of 140 degrees, a VFOV of 30 degrees, and an IFOV of 5 mrads. It has 105 columns and 490 rows. The edges correspond to contours of constant range of 30 meters, 60 meters, 90 meters etc.

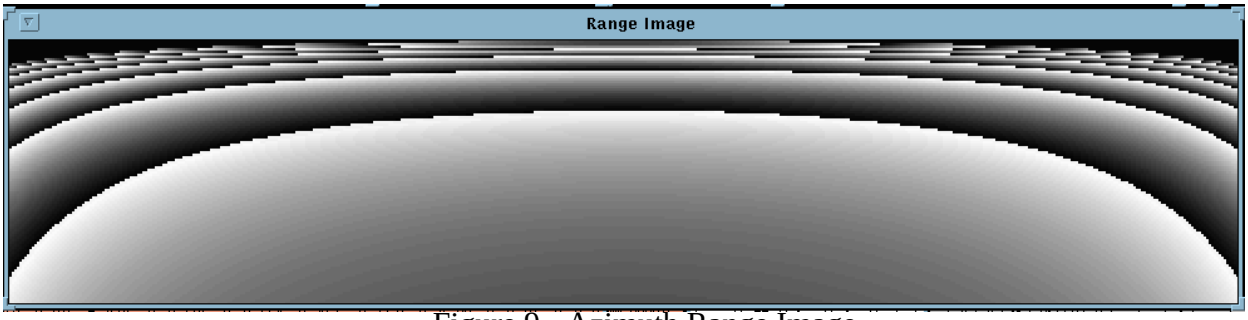

Figure 9 - Azimuth Range Image

The curvature of the contours of range is intrinsic to the sensor kinematics and is independent of the sensor tilt. Substituting this back into the coordinate transform, the coordinates where each ray intersects the groundplane are:

$$x_g = -ht\psi / s\theta\beta$$
$$y_g = h / t\theta\beta$$
$$z_g = 0$$

Notice that the y coordinate is independent of ψ and hence, lines of constant elevation in the image are ***straight lines along the y-axis*** on flat terrain.

6.2 The Field of View

Of basic interest is the region on the groundplane illuminated by the sensor. This can be computed in closed form as follows. From the previous result, it can be verified by substitution and some algebra that:

$$\left[\frac{x_g}{t\psi}\right]^2 - y_g^2 = h^2$$

Thus lines of constant azimuth are ***hyperbolas*** on the groundplane.

Let the two extreme columns of the image be given by the polar azimuth angles of $\pm\Psi$. Then, for the two extreme columns of the image given by $\psi = \pm\Psi$, the asymptotes of the hyperbola are of the form:

$$\frac{x_g}{t\Psi} = \pm y_g$$

Let the two extreme rows of the image be given by the polar elevation angles of $\pm\Theta$. Then the proximal and distal lines of the field of view are given by:

$$y_g = h / tan\,(\pm\Theta + \beta)$$

However, for most sensor tilt angles, the distal bound is far outside the sensor maximum range. Hence, the true limit of data is given by the intersection of a sphere centered at the sensor and the groundplane. By inspection, this sphere is given by:

$$x^2 + y^2 + h^2 = R^2_{max}$$

The shape of the field of view of a single image is given below:

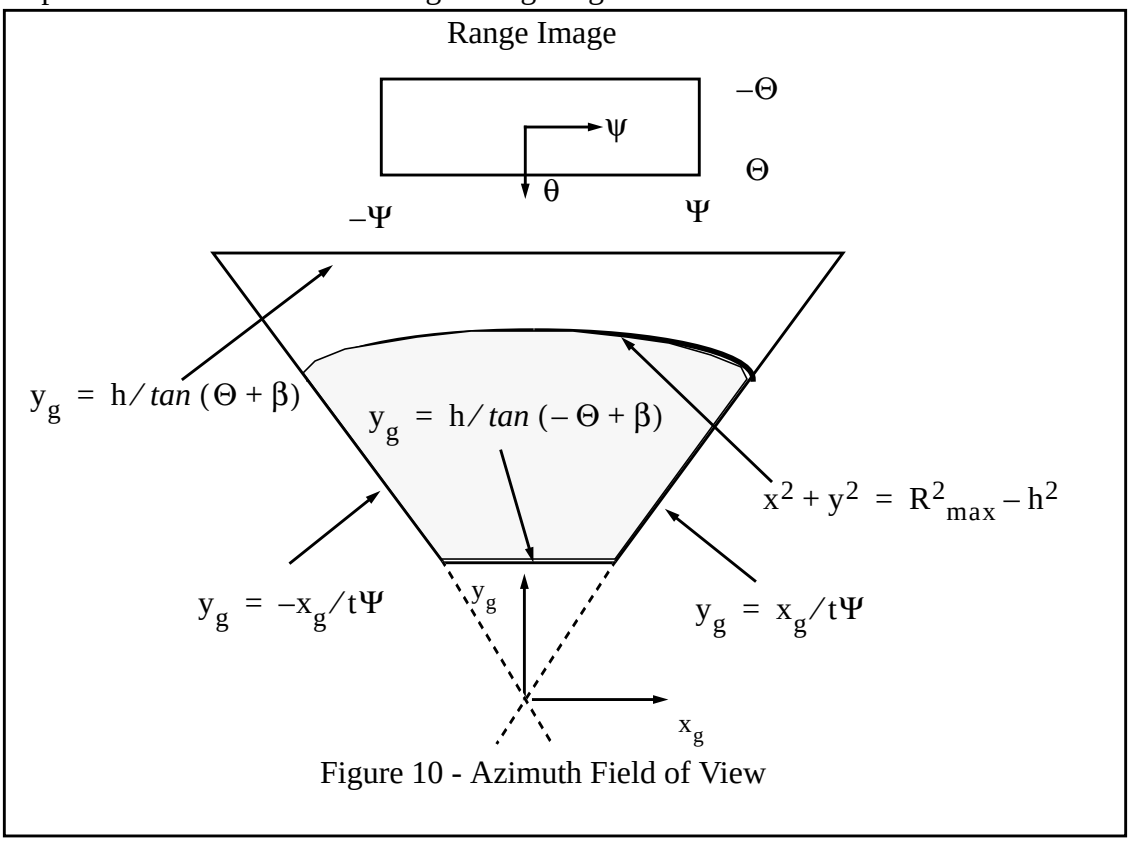

Figure 10 - Azimuth Field of View

6.3 Resolution

The Jacobian of the groundplane transform has many uses. Most important of all, it provides a measure of sensor resolution on the ground plane. Differentiating the previous result:

$$\begin{bmatrix} dx_g \\ dy_g \end{bmatrix} = \begin{bmatrix} \frac{h\,(sec\psi)^2}{s\theta\beta} & \frac{-ht\psi c\theta\beta}{(s\theta\beta)^2} \\ 0 & \frac{h}{(s\theta\beta)^2} \end{bmatrix} \times \begin{bmatrix} d\psi \\ d\theta \end{bmatrix}$$

The determinant of the Jacobian relates differential areas:

$$dx_g dy_g = \left[\frac{(h\,sec\psi)^2}{(s\theta\beta)^3} \right] d\psi d\theta$$

Notice that when R is large and $\psi = 0$, the Jacobian norm can be approximated by:

$$\left[\frac{(h\,sec\psi)^2}{(s\theta\beta)^3} \right] \approx h^2 / \left(\frac{h}{R} \right)^3 = R^2 / \left(\frac{h}{R} \right)$$

which is the same result given in [5].The scanning density is proportional to the cube of the range.

6.4 Azimuth Scanning Pattern

The scanning pattern is shown in the following figure with a 10 m grid superimposed for reference purposes. Only every fifth pixel is shown in azimuth to avoid clutter.

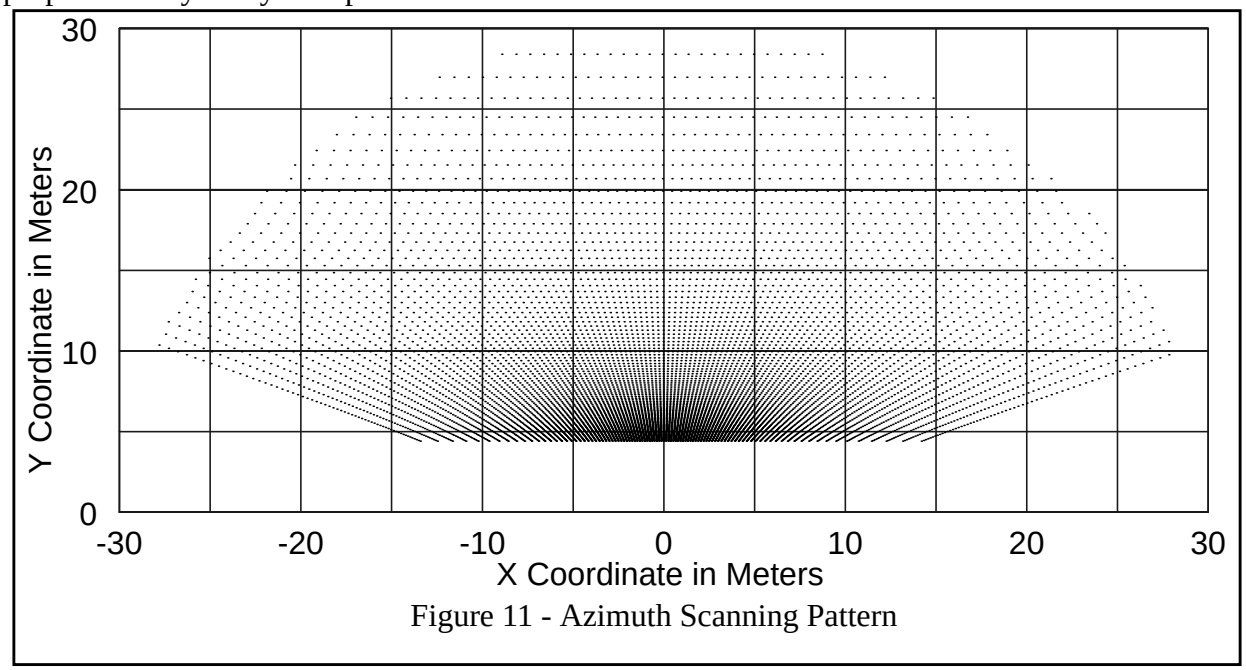

Figure 11 - Azimuth Scanning Pattern

6.5 Azimuth Spot Pattern

The spot pattern is obtained by intersecting the ground plane with the beam. Spots are shown at one tenth density in elevation and one seventh density in azimuth:

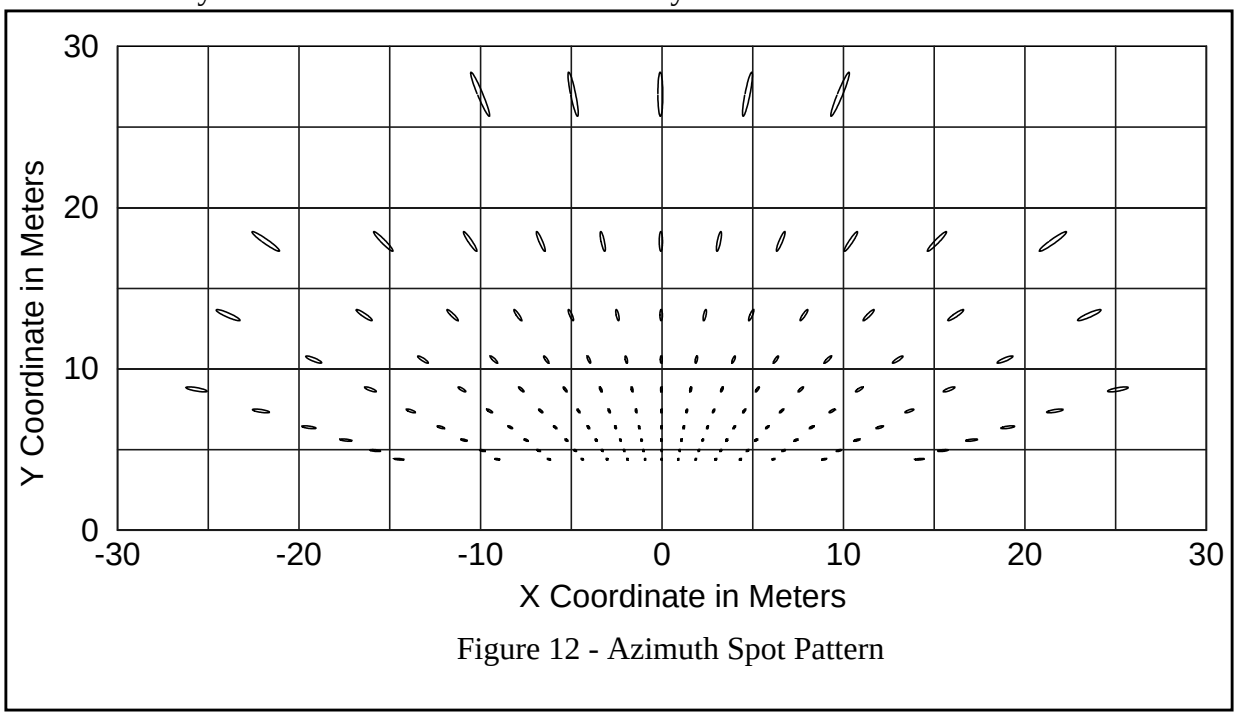

Figure 12 - Azimuth Spot Pattern

7. Kinematics of the Elevation Scanner

The **elevation scanner** is a generic name for a class of laser rangefinders with equivalent kinematics. In this scanner, the laser beam undergoes the elevation rotation/reflection first and the azimuth rotation/reflection second. It is the ***kinematic dual*** of the azimuth scanner. The Hurricane scanner falls into this category. While the Hurricane uses a single mirror actuated in two directions, equivalent kinematics can be generated in a dual mirror system in such a manner as to reduce by half the rotational speed of the mirrors. Consider a representative elevation scanner which is constructed by reconfiguring the ERIM scanner. Like the ERIM, this scanner is a 2D scanning laser rangefinder employing a "polygonal" mirror and a flat "nodding" mirror. Compared to the ERIM, the roles of the mirrors are reversed, and the order in which the beam encounters them is reversed. The mirrors move as shown below:

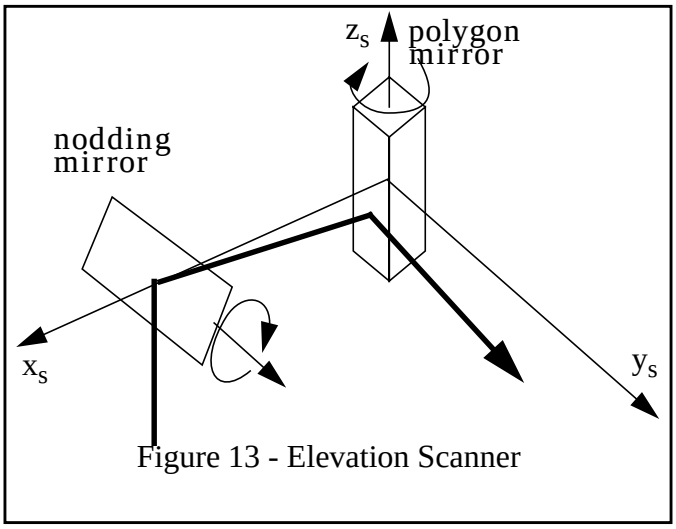

Figure 13 - Elevation Scanner

A coordinate system called the "s" system is fixed to the sensor with y pointing out the front of the sensor and x pointing out the right side. The beam enters along the z_s axis. It reflects off the nodding mirror which rotates about the y_s axis. It then reflects off the polygonal mirror, which rotates about the z_s axis, to leave the housing roughly aligned with the y_s axis.

First, the beam is reflected from the laser diode about the normal to the nodding mirror. Computation of the output of the nodding mirror can be done by inspection by noting that the beam rotates by twice the angle of the mirror because it is a reflection operation, and the z-x plane contains both the incident and normal vectors. The datum position of the mirror must correspond to a perfectly horizontal output beam, so the datum for the mirror rotation angle is chosen appropriately. Consider an input beam $\hat{v}_m$ along the z_s axis and reflect it about the mirror by

inspection:

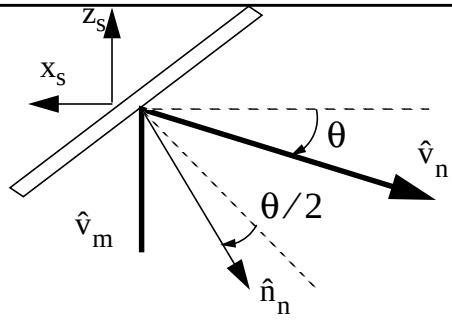

$$\hat{v}_m = \begin{bmatrix} 0 & 0 & 1 \end{bmatrix}^T$$

$$\hat{v}_n = \mathrm{Ref}(\hat{n}_n)\,\hat{v}_m$$

$$\hat{v}_n = \begin{bmatrix} -c\theta & 0 & -s\theta \end{bmatrix}^T$$

Figure 14 - Nodding Reflection

Notice that this vector is contained within the x_s-z_s plane. Now this result must be reflected about the polygonal mirror. Notice that, at this point, $\hat{v}_n$ cannot simply be rotated around the z axis since the axis of rotation which is equivalent to a reflection is normal to both $\hat{v}_n$ and $\hat{n}_p$. Since $\hat{v}_n$ is not always in the x_s-y_s plane, the z_s axis is not always the axis of rotation.

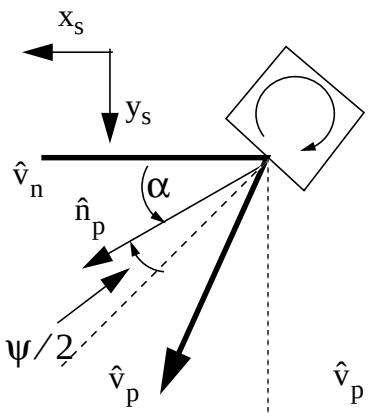

$$\hat{v}_n = \begin{bmatrix} -c\theta & 0 & -s\theta \end{bmatrix}^T$$

$$\text{put} \quad \frac{\alpha}{2} = \frac{\pi}{4} - \frac{\psi}{2}$$

$$\hat{n}_n = \begin{bmatrix} c\frac{\alpha}{2} & s\frac{\alpha}{2} & 0 \end{bmatrix}^T$$

$$\hat{v}_p = \mathrm{Ref}(\hat{n}_p)\,\hat{v}_n = \hat{v}_n - 2(\hat{v}_n \cdot \hat{n}_p)\,\hat{n}_p$$

$$\hat{v}_p = \begin{bmatrix} -c\theta \\ 0 \\ -s\theta \end{bmatrix} + 2c\theta c\frac{\alpha}{2}\begin{bmatrix} c\frac{\alpha}{2} \\ s\frac{\alpha}{2} \\ 0 \end{bmatrix} = \begin{bmatrix} c\theta c\alpha \\ c\theta s\alpha \\ -s\theta \end{bmatrix} = \begin{bmatrix} c\theta c\left(\frac{\pi}{2} - \psi\right) \\ c\theta s\left(\frac{\pi}{2} - \psi\right) \\ -s\theta \end{bmatrix}$$

$$\hat{v}_p = \begin{bmatrix} [c\theta s\psi] & [c\theta c\psi] & -[s\theta] \end{bmatrix}^T$$

Figure 15 - Polygonal Reflection

Which is the required result. This result is summarized in the following figure:

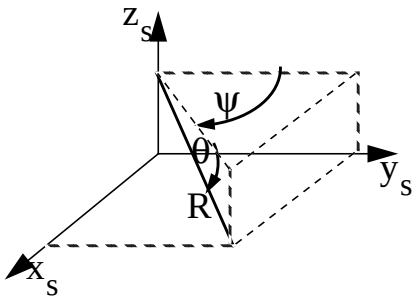

$$x_s = Rc\theta s\psi$$

$$y_s = Rc\theta c\psi$$

$$z_s = -Rs\theta$$

Figure 16 - Elevation Kinematics

In comparison to the azimuth scanner, the kinematics of the elevation scanner are equivalent to the same rotations taken in the opposite order. First, a rotation around the z_s axis followed by a rotation around the ***new*** x_s axis. By a theorem of 3D rotations, this is also equivalent to two rotations in the opposite order about fixed axes[3].

7.1 The Analytic Range Image of Flat Terrain

Given the basic kinematic transform, many analyses can be performed. The first is to compute an analytic expression for the range image of a perfectly flat piece of terrain. Let the sensor fixed "s"

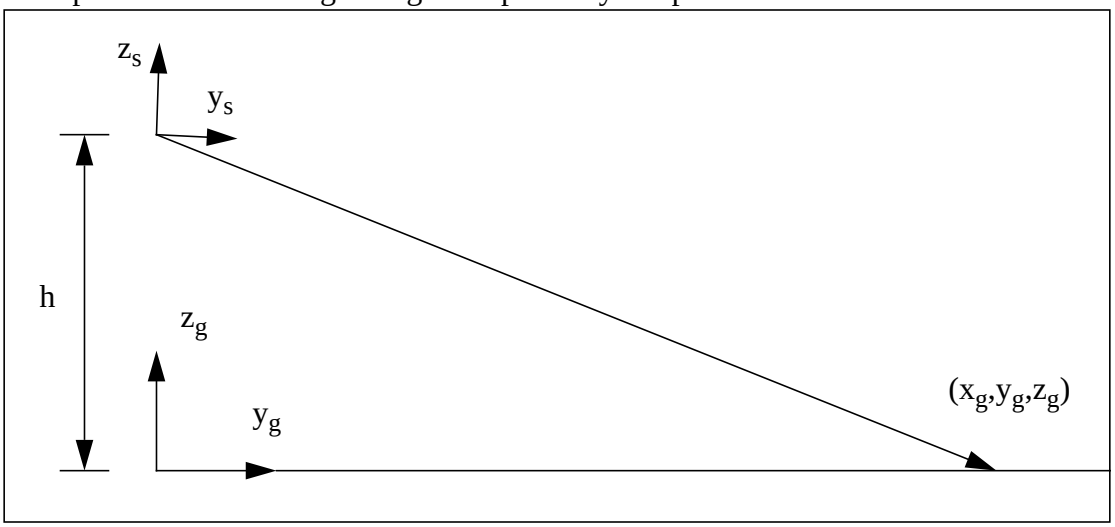

coordinate system be mounted at a height h. In the azimuth scanner, the sensor was tilted forward by an angle β. This was done to increase generality and cover the ERIM scanner as actually used on the HMMWV. It was easy to do because the elevation rotation was last in the azimuth scanner, so tilting the whole sensor was equivalent to tilting the nodding mirror a little more. In this case, the situation is reversed. While the mathematics of rolling the sensor are easy, they are of little use and the mathematics of pitching the sensor obscure the issues. Hence, for this scanner, a trivial

3. It is clear that there are only two possibilities for the order in which two rotations can take place about two orthogonal axes. Hence, there are **only two canonical forms** that the 2D laser rangefinder can take.

transform from sensor coordinates to global coordinates is considered:

$$x_g = x_s$$
$$y_g = y_s$$
$$z_g = z_s + h$$

However, a bias angle of β will be introduced into the nodding mirror. This will be the actual elevation angle of the center scanline of the image. Substituting the kinematics into this, the transform from the polar sensor coordinates to global coordinates is obtained:

$$x_g = Rc\theta\beta s\psi$$
$$y_g = Rc\theta\beta c\psi$$
$$z_g = h - Rs\theta\beta$$

Now by setting $z_g = 0$ and solving for R, the expression for R as a function of the beam angles ψ and θ for flat terrain is obtained. This is an analytic expression for the range image of flat terrain under the elevation transform.

$$R = h/s\theta\beta$$

Notice that in this case, $s\theta\beta = h/R$. This is the perception ratio defined earlier. As a check on the range image formula, the resulting range image is shown below for $h = 2.7$, $\beta = 16.5°$, a HFOV of 140 degrees, a VFOV of 30 degrees, and an IFOV of 5 mrad. It has 105 columns and 490 rows.

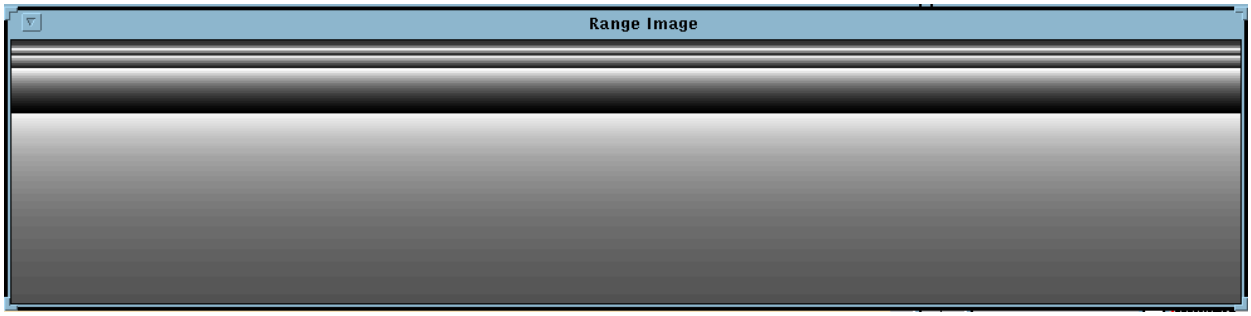

Figure 17 - Elevation Range Image

The edges correspond to contours of constant range of 30 meters, 60 meters, 90 meters etc. Notice that the contours do not approach the lower corners as they did in the azimuth scanner. Substituting this back into the coordinate transform gives the coordinates where each ray intersects the groundplane:

$$x_g = hs\psi/t\theta\beta$$
$$y_g = hc\psi/t\theta\beta$$
$$z_g = 0$$

Notice that the ratio x/y is $ht\psi$, which is independent of θ. Hence, lines of constant azimuth in the image are ***straight radial lines*** on flat terrain.

7.2 The Field of View

Of basic interest is the region on the groundplane illuminated by the sensor. This can be computed in closed form as follows. From the previous result, it can be verified by substitution and some algebra that:

$$[x_g]^2 + [y_g]^2 = \left(\frac{h}{t\theta\beta}\right)^2$$

Thus lines of constant azimuth are ***circles*** on the groundplane.

Let the two extreme columns of the image be given by the polar azimuth angles of $\pm\Psi$. Then the equations of the two lines which bound the field of view are:

$$y_g = \pm\frac{x_g}{ht\Psi}$$

Let the two extreme rows of the image be given by the polar elevation angles of $\pm\Theta + \beta$. Then the radii to the proximal and distal circles of the field of view are given by:

$$R = h / tan\,(\pm\Theta + \beta)$$

If this distal bound is far outside the sensor maximum range, then the maximum range is the radius of the far circle. In this case, the true limit of data is given by the intersection of a sphere centered at the sensor and the groundplane. By inspection, this sphere is given by:

$$x^2 + y^2 + h^2 = R^2_{max}$$

The shape of the field of view of a single image is given below:

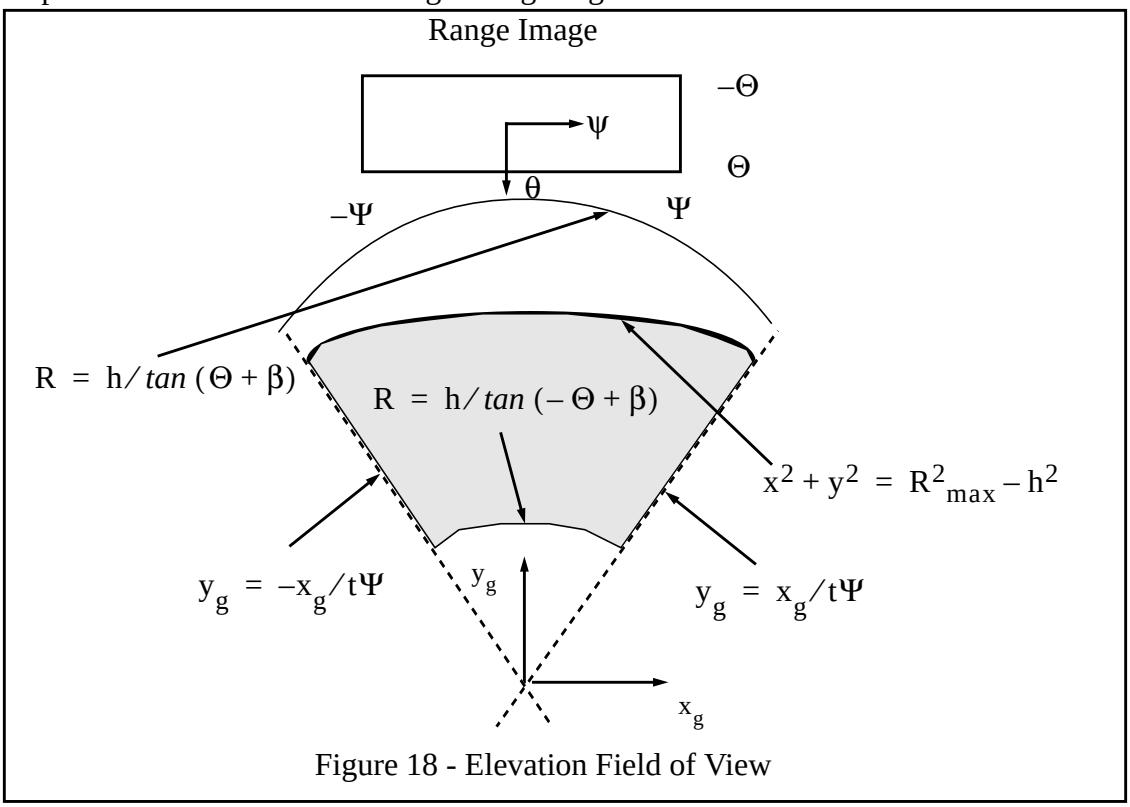

Figure 18 - Elevation Field of View

7.3 Resolution

The Jacobian of the groundplane transform has many uses. Most important of all, it provides a measure of sensor resolution on the ground plane. Differentiating the previous result:

$$\begin{bmatrix} dx_g \\ dy_g \end{bmatrix} = \begin{bmatrix} \frac{hc\psi}{t\theta\beta} & \frac{h\,[s\psi\,sec^2\theta - c\psi t\theta\beta]}{t^2\theta\beta} \\ \frac{-hs\psi}{t\theta\beta} & \frac{h\,[c\psi\,sec^2\theta + s\psi t\theta\beta]}{t^2\theta\beta} \end{bmatrix} \times \begin{bmatrix} d\psi \\ d\theta \end{bmatrix}$$

The determinant of the Jacobian relates differential areas:

$$dx_g dy_g = \left[\frac{(h\,sec\psi)^2}{(t\theta\beta)^3}\right] d\psi d\theta$$

which is identical to the azimuth Jacobian norm except that the denominator is a tangent instead of a sine. Notice that when R is large or small and $\psi = 0$, the Jacobian norm is:

$$\left[\frac{(h\,sec\psi)^2}{(t\theta\beta)^3}\right] = h^2 / \left(\frac{h}{R}\right)^3 = R^2 / \left(\frac{h}{R}\right)$$

which is the same result given in [5]. Scanning density is cubic in range.

7.4 Elevation Scanning Pattern

The scanning pattern is shown in the following figure with a 10 m grid superimposed for reference purposes. Only every fifth pixel is shown in azimuth to avoid clutter.

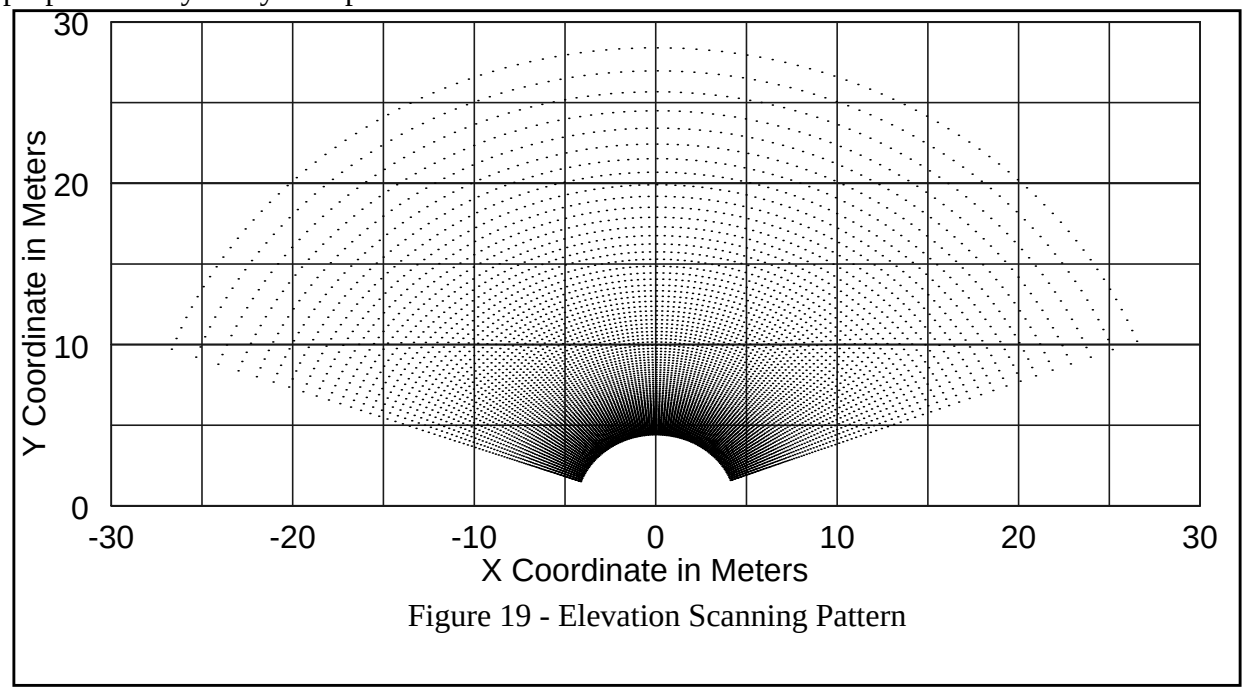

Figure 19 - Elevation Scanning Pattern

7.5 Elevation Spot Pattern

The spot pattern is obtained by intersecting the ground plane with the beam. Spots are shown at one tenth density in elevation and one seventh density in azimuth:

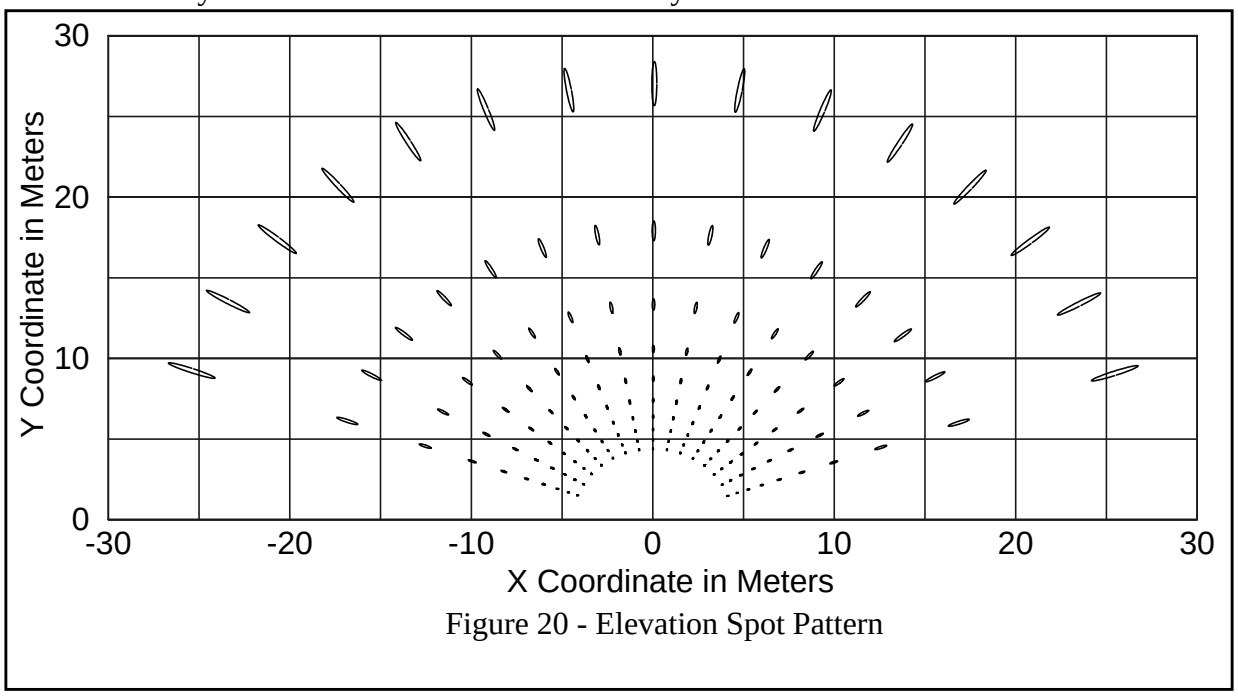

Figure 20 - Elevation Spot Pattern

8. Scanning Mechanism

This section covers some of the basic tradeoffs involved in the design of a rangefinder scanning mechanism. Much of this information is a result of the work of Dan Christian which has been recast in the format of this report. A dual mirror scanner will be considered, but few of the results depend on this. Let the highest speed mirror be called the **primary** and the low speed mirror is then called the **secondary**. Further, let the mirror closest to the optics be called the **internal** and the one farthest from the optics is then called the **external**.

This section on mechanism tradeoffs was written in consultation with Dan Christian.

8.1 Throughput/ Mirror RPM Tradeoff

For **uniform polar scan**, the IFOV gives not only the width of the beam but also the space between pixels. For the primary mirror, the beam must rotate at sufficient angular rate to move the beam an angular distance of the IFOV over the time between pulses. Hence, for a mirror gain of K_M, the governing relationship is as follows:

$$f_{mirror} = \frac{f_{pixels}\left(\frac{pixels}{sec}\right) \times IFOV\left(\frac{rads}{pixel}\right)}{K_M} = \frac{f_{pixels} IFOV}{K_M}$$

If this expression is converted to units of rpm:

$$f_{mirror} = \frac{f_{pixels}\left(\frac{pixels}{sec}\right) \times IFOV\left(\frac{rads}{pixel}\right) \times 60\left(\frac{sec}{min}\right)}{2\pi\left(\frac{rads}{rev}\right)K_M} = \frac{60 f_{pixels} IFOV}{2\pi K_M}\left(\frac{rev}{min}\right)$$

Notice that mirror speed depends on the ***gross*** laser bandwidth. This relationship is independent of the effective number of facets in the mirror because mirror facets cause the field of view to be folded back on itself while maintaining the same angular rate of the beam. This relationship is plotted in the following figure:

Notice that the angular speed of mirrors required for high pulse rates quickly becomes unreasonable unless the IFOV is reduced. However, reduced IFOV also reduces either the field of view or the frame rate, so it is necessary to choose the IFOV very carefully.

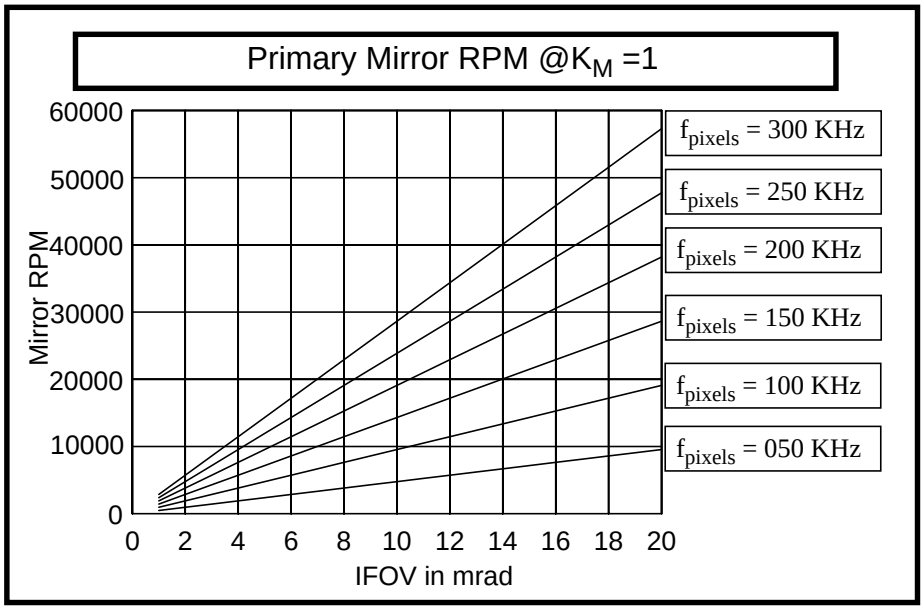

Figure 21 - Mirror RPM

8.2 Duty Cycle / Mirror Size Tradeoff

The **duty cycle** η_T is a number less than 1 which expresses the loss of bandwidth which occurs when the laser is not being used while mirrors are moved into position. In a two mirror system, a duty cycle can be defined for each mirror such that the overall duty cycle is the product of the two. For nodding type mirrors, the duty cycle is related to the rise time of the speed servo which drives the mirror, and the field of view generated.

For polygonal mirrors, the duty cycle is related to the field of view generated by the mirror, the size of the receive optics, and the size of the mirror itself. Consider a polygon mirror constructed by inscribing a regular polygon inside a circle. It is clear that each facet subtends an angle α that depends only on the number of facets n. Also, a simple expression for the length of each facet in terms of the diameter of the circumscribing circle is available:

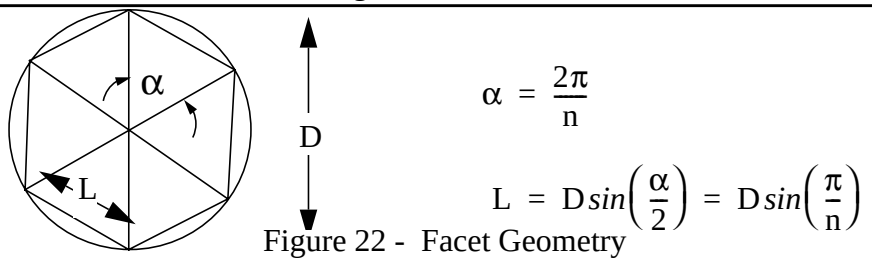

Figure 22 - Facet Geometry

The largest possible field of view obtainable from a facet is related to the mirror gain and the total number of facets. The angle scanned by the beam is the mirror gain times the angle moved by the mirror. The maximum possible angular motion of the mirror is the angle subtended by a facet, since, at this point, the next facet moves into position occluding the previous. The governing

relationship is therefore:

$$FOV_{ideal} = K_M \alpha = K_M \frac{2\pi}{n}$$

Thus, the field of view can be doubled by entering the mirror in the optimal direction, but is reduced linearly with the number of facets. In practice, the field of view can be considered a fixed requirement, and the design problem is to choose the number of facets which is consistent with this.

8.2.1 Corner Loss

Let the diameter of the receive optics be given by d. In a realistic case, the corners of the polygon cause a loss of effective bandwidth. This will be called the **corner loss**. This chopping of a portion of the receive beam is also known as **vignetting**. The laser cannot be used over some fraction of the angle subtended by the receive optics as shown below:

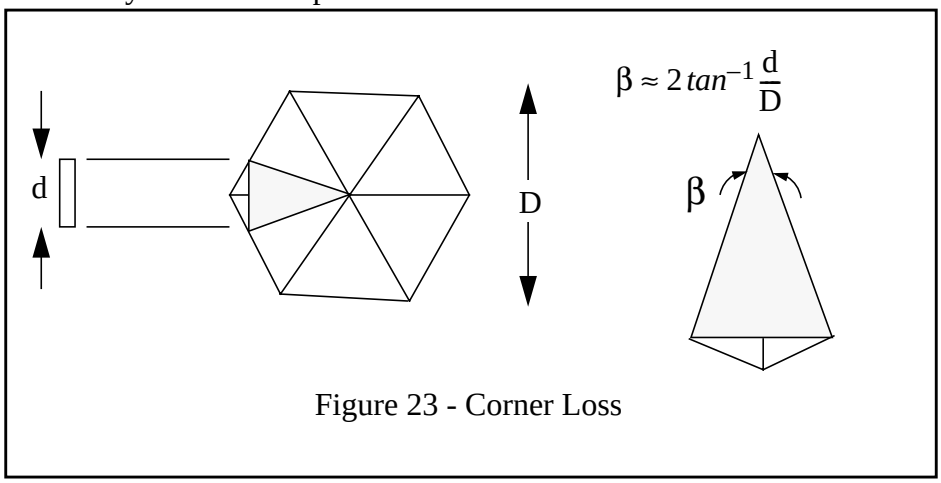

Figure 23 - Corner Loss

This analysis assumes the best possible case where the third dimension is used to allow transmit and receive along the same axis in the plane without interference. Incorporating the corner loss, the maximum field of view obtainable is given by:

$$FOV_{max} = FOV_{ideal} - \beta = K_M \frac{2\pi}{n} - 2\,tan^{-1}\frac{d}{D}$$

In practice, it is possible to accept some degradation in signal to noise ratios by using the mirrors in regions where part of the corner is subtended. The amount to which this is possible depends on the permitted degradation in signal to noise ratio. Complete elimination of corner loss requires mirrors of infinite size, so some amount must be accepted.

The four faceted polygonal mirror of the ERIM could potentially generate a 180 degree horizontal field of view. The reason for the small 80 degree field of view is the limited size of the nodding mirror.[4]

8.2.2 Rounding Loss

The number of facets used in a polygonal mirror must be an integer. Therefore, if the required field

4. From Dave Zuk of the Environmental Research Institute of Michigan.

of view is not some integral fraction of a total rotation times the mirror gain, data is being wasted because the field of view is not optimally folded. In practice, this **rounding loss** can be easily eliminated by appropriate choice of the field of view. As a general rule, if polygonal mirrors are used, the associated field of view should be increased as far as is possible toward the angle subtended by each facet because the laser will otherwise have to wait for the mirror anyway. For a field of view that is not a complete circle, a polygonal mirror is necessary to reduce this loss to a minimum. The following table summarizes the possibilities for field of view:

Table 1: Optimal Field of View

n	FOV @ K_M=1	FOV @ K_M=2
1 (planar)	360 degrees	720 degrees
2	180 degrees	360 degrees
3	120 degrees	240 degrees
4	90 degrees	180 degrees
5	72 degrees	144 degrees
6	60 degrees	120 degrees

8.2.3 Duty Cycle

The **duty cycle** is now easy to express as the ratio of the usable field of view to the ideal field of view:

$$\eta_T = \frac{FOV}{FOV_{ideal}}$$

When the rounding loss is eliminated, the duty cycle can be expressed as:

$$\eta_T = \frac{FOV_{ideal} - FOV_{loss}}{FOV_{ideal}} = \frac{K_M \frac{2\pi}{n} - 2\,tan^{-1}\frac{d}{D}}{K_M \frac{2\pi}{n}} = 1 - \left(\frac{n}{\pi K_M}\right) tan^{-1}\frac{d}{D}$$

This relationship is plotted below as a function of the ratio of diameters of the receive optics and the mirror circumscribing circle. Efficiency decreases with the number of facets because more facets imply that the length of each facet is smaller relative to the receiving aperture.

Current rangefinders employ roughly 2 inch aperture receive optics. Under a limitation of a maximum mirror diameter of, say, 8 inches, a 6 facet mirror will have a duty cycle of 0.75 according to this graph. If both primary and secondary mirrors have roughly equivalent duty cycles, ***it is not hard to see that the overall laser utilization can easily drop near 50% unless special measures are taken to avoid bandwidth loss***. In practice, some amount of vignetting is tolerated in order to reduce this loss.

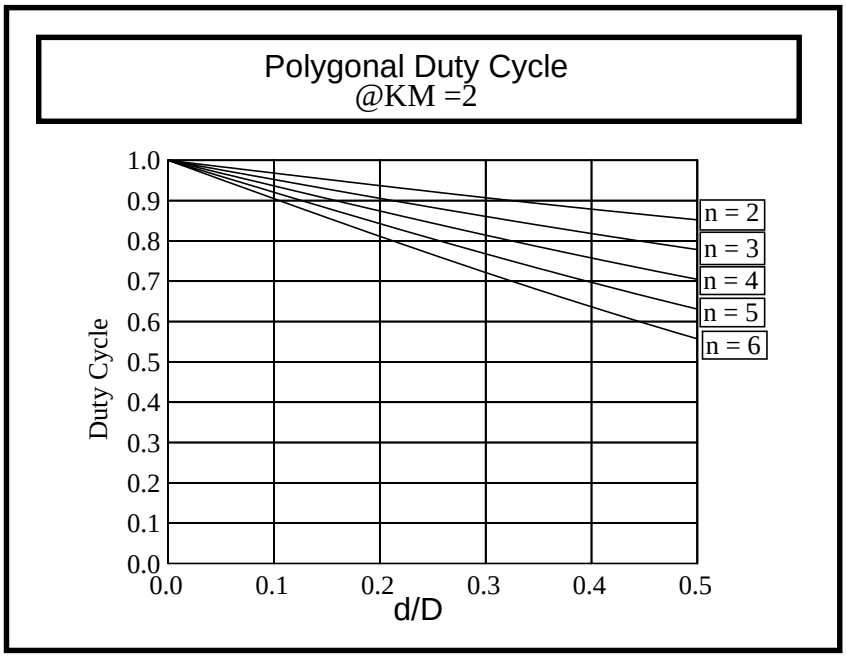

Figure 24 - Duty Cycle

8.3 Field of View / Mirror Size Tradeoff

In systems employing two mirrors, the internal mirror need only be large enough to subtend the area of the receive optics over its complete range of rotation. The required size of the external mirror, however, can rapidly grow with the field of view to unreasonable proportions. Considering the ERIM case as an example, the relationship which governs the length of the nodding mirror is given below:

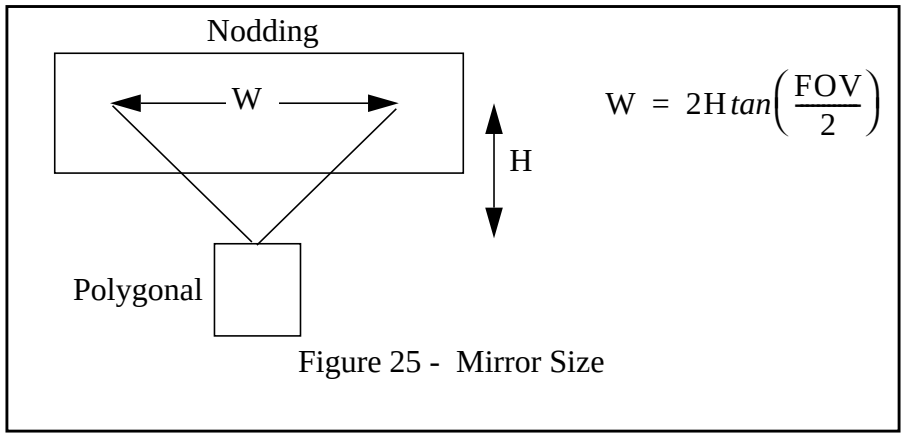

Figure 25 - Mirror Size

In the case of the ERIM, the perpendicular separation H of the mirror axes was chosen such that the nodding mirror was free to rotate completely around without colliding with the polygonal mirror. As the field of view increases however, it becomes necessary to reduce H in order to keep the width W reasonable.

8.4 Speed / Resolution / Field of View Tradeoff

The **laser bandwidth** is a sensor performance parameter of extreme importance. Intuitively, it represents the rate at which geometric information can be acquired in range measurements per second. Clearly, because the field of view is comprised of some number of pixels in azimuth and elevation, the frame rate is limited to be the laser bandwidth divided by the number of pixels in an image.

More generally, consider a 2D scanner in which the azimuth mirror is the primary. If HFOV is the horizontal field of view, VFOV is the vertical field of view, IFOV is the beam dispersion or "instantaneous" field of view, η_T is the aggregate laser duty cycle accounting for all losses, f_{images} is the **frame rate**, and f_{pixels} is the **laser pulse rate** (aka **sensor throughput** or **laser bandwidth**), then the basic design problem is to allocate pixels optimally over the field of view subject to the constraint that:

$$f_{pixels}\left(\frac{pixels}{sec}\right)\times\eta_T = \frac{HFOV}{IFOV}\left(\frac{pixels}{line}\right)\times\frac{VFOV}{IFOV}\left(\frac{lines}{image}\right)\times f_{images}\left(\frac{images}{sec}\right)$$

The **net sensor throughput** is numerically equivalent to the laser pulse rate times the duty cycle. In the design tradeoffs, it is possible to increase either or both of the field of view and the frame rate provided an appropriate decrease in resolution is suffered to compensate.

It is useful to define the **line rate** as the frequency at which horizontal lines are acquired. The line rate is a convenient parameter for comparing different sensors. It is defined as follows:

$$f_{lines} = \frac{VFOV}{IFOV}\left(\frac{lines}{image}\right)\times f_{images}\left(\frac{images}{sec}\right) = \frac{f_{pixels}\left(\frac{pixels}{sec}\right)\times\eta_T}{\frac{HFOV}{IFOV}\left(\frac{pixels}{line}\right)}$$

Notice that the line rate depends on the **net** laser throughput. If the duty cycle is determined solely by the HFOV, the expression can be rewritten by replacing:

$$\frac{HFOV}{\eta_T} = HFOV_{ideal} = \frac{K_M 2\pi}{n}$$

This can be expressed in more meaningful units of degrees per second by multiplying by the number of degrees per line, which is the IFOV. This gives the **vertical sweep rate**. For a uniform polar scan, the vertical sweep rate is quadratic in IFOV:

$$\dot{\theta} = \frac{f_{pixels}\left(\frac{pixels}{sec}\right)\times\eta_T}{\frac{HFOV}{IFOV}\left(\frac{pixels}{line}\right)}IFOV\left(\frac{rads}{line}\right)\times\frac{180}{\pi}\left(\frac{degrees}{rads}\right)$$

This relationship is plotted below. ***The quadratic dependence on IFOV makes increased angular resolution very costly to the sweep rate***. For the sweep rate, the convenient relationship is

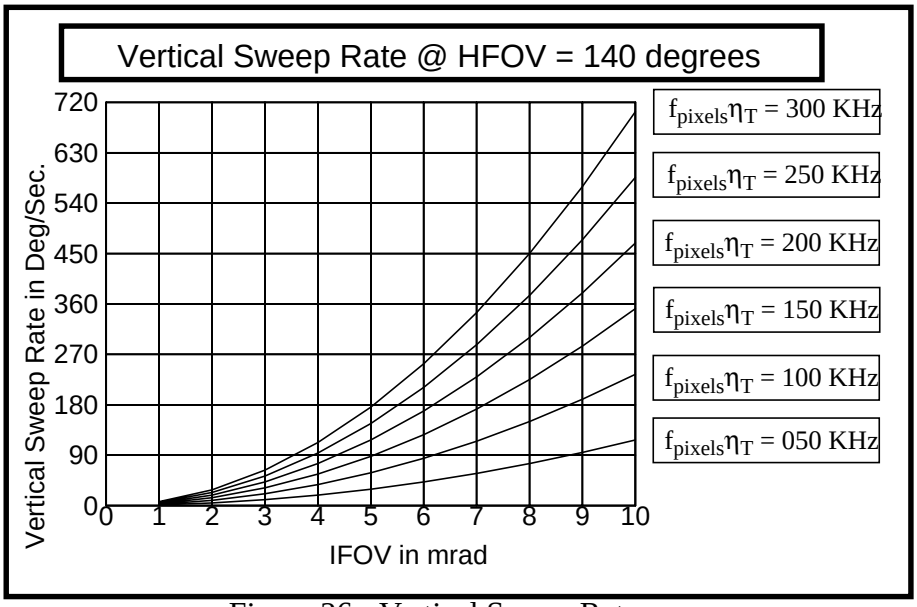

Figure 26 - Vertical Sweep Rate

available:

$$VFOV\left(\frac{degrees}{image}\right) = \dot{\theta}\left(\frac{degrees}{sec}\right) / f_{images}\left(\frac{images}{sec}\right)$$

8.5 Summary

This section has established the following:

- Mirror rpm is determined solely by the gross laser bandwidth, the mirror gain, and the beam dispersion. Large beam dispersions cannot be achieved with high bandwidth lasers while preserving reasonable mirror angular velocity.
- Some amount of bandwidth loss due to vignetting must be accepted for polygonal mirrors. Increased mirror size relative to the receiving aperture reduce this loss.
- A small discrete set of values for the field of view are optimal from the point of view of laser duty cycle.
- Laser utilization can easily drop close to 50% unless special measures are taken to prevent it.
- The size of the secondary mirror can grow to unreasonable proportions for wide field of view sensors unless the mirrors are packaged closely.
- Finite laser bandwidth gives rise to a basic tradeoff between speed, resolution, and field of view of any rangefinder.
- Sweep rate grows quadratically with beam dispersion. Therefore, increased obstacle resolving power is very costly to the sweep rate.

9. The Ideal Cartesian Scanner

The next three sections consider the design options for a laser scanner in a quantitative manner. The major requirements imposed by the vehicle on the scanner are as follows:

- 1/6 m map resolution
- ability to detect a 1/6 m step obstacle at the maximum range

The reaction time and maximum velocity can be traded against other design parameters if necessary. The driving component performance parameters are as follows:

- laser pulse throughput cannot exceed 200 KHz
- laser beam divergence must be in the range 2 mrad to 10 mrad
- angular velocity of mirrors cannot exceed 10,000 rpm

The idea of **uniform cartesian scan** is to modulate the IFOV and the interpixel spacing in such a way as to maintain a constant spot size, shape, and spacing over the ground plane for flat terrain. This section considers the requirements for such a scanner.

9.1 Requirements Summary

It was shown in [5] that in order to optimally support 20 m.p.h. speeds for the worst case of reaction times considered, an ideal rangefinder would meet the following requirements:

Table 2: Requirements for Ideal Uniform Cartesian Sensor

Requirement	Value
Groundplane Resolution	1/6 meter
Throughput	300 KHz
Maximum Range	65 meters
HFOV	240 degrees
VFOV	+/- 30 degrees
IFOV	variable

According to Figure 49 of [5], such a sensor would require 15 Mflop geometric processing power. This is almost a feasible number because of the cartesian uniformity of the scanning density. Such a sensor would, by placing pixels optimally on the ground, make it feasible to process an entire image at appropriate resolution. Note that the “image” generated by such a sensor has the same shape as the projection of the field of view onto the groundplane, which is roughly a trapezoid.

9.2 Infeasibility of the Uniform Cartesian Scanner

While such a rangefinder is nearly ideal compared to existing scanners, it must be eliminated from consideration on the following grounds:

9.2.1 IFOV Modulation

As well as controlling the speed of the laser scan, it is also necessary to modulate the IFOV to be equal to the pixel angular spacing in order to ensure that one range reading really does correspond to the range in a single map cell. It is clear from Figure 2 that for a map resolution of 1/6 meter, this requires that the IFOV vary over a very significant range. Dimensional analysis in [5] has shown that the IFOV must vary by the square root of the cube of the ratio of maximum to minimum range. Further, the modulation function must cycle at frame rate. Technology to actively control IFOV by dynamic beam collimators is apparently not available.

If the dispersion of the beam is modulated equally in azimuth and elevation, then the spots will have the correct size on the ground but not the correct aspect ratio. Correcting the aspect ratio requires another degree of freedom in the collimation which must also cycle at frame rate. Dimensional analysis has shown that the variation in aspect ratio over the ground plane is the ratio of maximum to minimum range. The aspect ratio itself is given by the **perception ratio**.

9.2.2 Singularity and the Flat Terrain Assumption

The scanning rates and IFOV for uniform cartesian scan are based on an assumption that the terrain is flat. For a vertical field of view that includes the horizontal, mirror velocities near the horizontal tend to zero. Therefore, cartesian position of the spot is extremely sensitive to the elevation mirror position to the point when mirror control may be infeasible. Also, there is no basis for deciding on the elevation mirror rates above the horizon.

9.2.3 Mirror RPM

Just as mirror rates tend to zero at the horizon, they tend to infinity close to the vehicle. Based upon a resolution of 1/6 meter (16 cm), Figure 2 gives, on extrapolation, an instantaneous IFOV of about 25 mrad at the minimum range. Based on this figure, a throughput of 200 KHz, and a mirror gain of 1, Figure 21 gives an angular velocity of the primary mirror of 45,000 rpm which is a ***very*** difficult speed to achieve.

9.3 Summary

This section has established the following:

- The primary reason for rejecting the uniform cartesian scanner is the IFOV modulation problem. Assuming it could be solved, it is likely that practical solutions to the remaining problems could be found. After all, this concept is an extreme on a continuous spectrum. Even if completely uniform cartesian scan is infeasible, a scanner which is ***less nonuniform*** can certainly be constructed using IFOV modulation.

10. The Ideal Polar Scanner

Having rejected an uniform cartesian scanner, this section considers the requirements which would be placed upon a more traditional uniform polar scanning sensor. In **uniform polar scan**, the interpixel spacing equals the IFOV in each direction. Many variations are possible by varying the beam aspect ratio and the interpixel spacing unequally in elevation and azimuth. For the balance of the section, however, ***it is assumed that beam dispersion equals interpixel spacing*** so that 100% coverage of the environment is achieved. Further, it is assumed that ***the beam is circular in cross section***.

10.1 Requirements Summary

It was shown in [5] that, in order to optimally support 20 m.p.h. speeds for the worst case of system reaction times considered, an ideal uniform polar scanning rangefinder would meet the following requirements:

Table 3: Requirements for Ideal Uniform Polar Sensor

Requirement	Value
Groundplane Resolution	variable, no greater than 1/6 meter
Throughput	determined by FOV and frame rate
Maximum Range	65 meters
HFOV	240 degrees
VFOV	+/- 30 degrees
IFOV	0.5 mrad

The IFOV requirement comes from Figure 2 by insisting on landing six pixels on a vertical step obstacle that is six inches high at 50 meters range. Such a sensor would require a laser pulse rate of 13.44 MHz. Hence, such a sensor is beyond current technology if a uniform polar scan with fixed IFOV is accepted. Further, the processing and communications bandwidth requirements are 700 Mflops and 134 MHz. Such processing rates are approached only by today's supercomputers.

10.2 Summary

This section has established the following:

- A uniform polar scanner cannot be constructed which meets all system requirements, and even if it could, existing computer processing power is insufficient.

11. A Practical Scanner - The Tornado Concept

This section proposes a compromise of specifications for a practical laser scanner.

11.1 Field of View

11.1.1 Implications of Finite Computing Resources

Analysis from [5] has shown that the sensor maximum range increases as either reaction time or vehicle speed increases. It has also shown that increased range requires that the IFOV be reduced in order to resolve obstacles.

Therefore, the rest of this section will assume a 1 second braking reaction time, and a 2 second turning reaction time[5]. It is this assumption which permits reduction of the maximum sensor range, the horizontal field of view, and the sensor angular resolution.

From Figure 16 of [5], the required maximum range is then 45 meters and, from Figure 18 of [5], the required horizontal field of view is 100 degrees. This will be increased to 120 degrees to reduce rounding loss and to introduce some margin into the assumed coefficient of friction in the turning stop maneuver.

There is a second reason for assuming a 2 second reaction time other than the limitation in laser bandwidth and processing power. If the sensor is mounted on the vehicle roof, such a slow reaction time leads to a violation of the **minimum acuity** rule. From Figure 16 of [5], a 4 second reaction time requires a maximum range of 65 meters at 10 meters/sec speeds. Using the HMMWV wheelbase of 3.3 m, the sensor height of 2.7 m, and a range of 50 meters, the acuity rule gives a maximum beam dispersion of 1.0 mrads.

As a verification of this, consider the dy graph of Figure 2. It is clear that at 50 meters, most values of the beam dispersion give unreasonable pixel spacings at the maximum range. Over the range of beam dispersions available today, the data that can be generated at high ranges is useless anyway, so the only way to solve the acuity problem is to reduce the maximum range. For given terrain and a given speed goal, this can only be accomplished by reducing the reaction time.

11.1.2 Implications Resolution / Speed Tradeoff

One consideration which argues for a narrow vertical field of view is the tradeoff of resolution for speed. To adopt a wide vertical field of view is to adopt reduced angular resolution through the limitation of the laser bandwidth. This approach is doubly unsound. First, it sacrifices obstacle resolving power at high ranges unreasonably in favor of dubious ability to detect obstacles near the vehicle at high speed. Second, it is justified based on a kinematic argument for very rough terrain which can probably not be negotiated for other reasons.

---

5. Part of the reason for this large turning reaction time is that rollover dynamics limit the steering rate to levels which are as yet unknown. Intuitively, it seems unsafe to turn a steering wheel through full deflection in a couple of seconds at high speeds.

11.2 Angular Resolution

11.2.1 Implications of the Spot Aspect Ratio

Earlier design iterations traded sweep rate for angular resolution and ended up with, basically, a better ERIM. However, the implications of the sweep rate rule and the spot rules on scanning efficiency were later recognized because such a sensor generated unreasonably poor scanning efficiencies.

To accept high depression (30 degree) scanlines in the field of view is to accept a **range ratio** of about 10 and hence ***a factor of 1000 variation in scanning density*** using a 45 meter maximum range. On this basis, roughly only 1 pixel in 1000 would be useful at the minimum range if angular resolution at the maximum range were optimal. The scanning density variation with the ERIM is about 64 which is already very wasteful, but the growth of this waste with range is cubic and simply cannot be tolerated in a new sensor, given that computational throughput is already a limiting factor.

11.2.2 Implications of the Scanning Efficiency

A wide vertical field of view also causes unreasonable imaging densities. If the lower scanline is 30 degrees depression, ***the imaging density at 10 m.p.h. is 16***. On this basis, about one image in 10 is useful, and the rest are waste.

Summarizing these last two points: if the new scanner were configured as the ERIM currently is, only one pixel in 10,000 would provide useful information at certain positions in the field of view. The scanning efficiency close to the vehicle in the center of the field of view would be 0.01%. A single scanline sensor can achieve a scanning efficiency of 100% if properly configured[6]. ‘

This is the basic lesson of the complexity analysis of [5] in concrete form. At high speeds, the **hole occlusion rule** cannot be satisfied anyway, so there is no point in having high depression pixels. On this basis, ***any high speed rangefinder must adopt a narrow vertical field of view*** unless extraordinary bandwidth waste is accepted. This holds equally for stereo systems.

11.2.3 Implications of the Acuity Rules

The minimum acuity rule is as follows:

$$d\theta = \frac{1}{2}\left(\frac{L}{R}\right)\left(\frac{h}{R}\right)$$

Based on a 45 meter maximum range, the minimum acuity rule gives a maximum IFOV of 2.2 mrads. Beyond this angular resolution, the data at the extremes of the image is useless. Based on this consideration, a 2 mrad beam dispersion is chosen. For a 120 degree HFOV, this gives 1050 pixels per line.

6. This is very likely the reason for the phenomenal success of the FASTNAV system.

Based on this, Tornado still cannot resolve small obstacles at the maximum range, but it is still 5 times better than the ERIM. The maximum acuity rule is as follows for an **oversampling factor** of 3:

$$d\theta = \frac{1}{6}\left(\frac{r}{R}\right)$$

which gives a required dispersion of 1.2 mrads. So Tornado is also pretty close to meeting this constraint. This happens because the two constraints converge just beyond the maximum range.

11.3 Other Specifications

The Tornado concept emerges from these considerations. It is a narrow VFOV sensor with a high performance programmable vertical scan and high angular resolution. However difficult it is to control such a scan, the problem must be addressed because it is the only solution to the problem until it becomes feasible and cost effective to generate pipelined gigaflops on a mobile platform. The design rationale is as follows:

- choose an angular resolution consistent with step obstacle detection at the maximum range
- choose a horizontal field of view consistent with vehicle maneuverability at all speeds up to 20 m.p.h.
- choose the instantaneous VFOV based on the laser bandwidth but allow 60 degrees of physical motion
- verify that mirror rpm and imaging densities remain feasible

The sensor which emerges from these considerations has all of the advantages of a single line scanner but none of the disadvantages. Its scanning efficiency is much higher. It permits considerably more robust obstacle detection and higher vehicle speeds. It permits map matching as a form of position estimation update.

11.3.1 Sweep Rate

At this point, it has been argued that a speed goal of 10 m/s requires a 2 second turning reaction time using existing rangefinder technology. The next matter to be considered is the sweep rate achievable at the acuity limit. Although a gross pulse rate of 200 KHz is achievable, it is practical to accept that at least 25% of this bandwidth will be wasted because a duty cycle above 0.75 is very difficult to achieve. A 150 KHz net pulse rate corresponds to 140 lines per second. From Figure 21, for a **net** pulse rate of 150 KHz, the achievable sweep rate at 2 mrad IFOV is a mere 16 degrees per second. Compared to the ERIM sweep rate of 60 degrees per second, there appears to be a problem. However, there is no problem because pointing the sensor farther downrange permits a small VFOV to still project onto a reasonable distance.

In order to be consistent with a high performance vehicle, frame rates on the order of 4 Hz are necessary. With such a choice of frame rate, the VFOV is only 4 degrees. However, when the top scanline is placed at 45 meters range, the bottom falls at about 20 meters. This gives a range ratio of 2.25. On this basis, scanning density varies by about 10 over a single image. This is six times better than the ERIM. Imaging density in this configuration is also 10. Imaging density decreases as the VFOV is pointed downward, so this leaves some margin for slower speed work.

On this basis, scanning efficiency is increased by a factor of 100 over the worst case generated by a choice of vertical field of view based on kinematic arguments.

11.3.2 Programmable Vertical Scan

In practice, 60 degrees of vertical motion (30 above and 30 below the horizon) of the elevation mirror will be permitted, and the vertical scan will be programmed in order to permit trading off the VFOV against frame rate in a different manner for each application. More importantly, a programmable VFOV permits stabilization which becomes more necessary as the maximum range is increased. The stabilization loop must servo the groundplane y coordinate. In order to do this, the loop must be closed after the sensor and vehicle kinematic transforms.

11.3.3 Primary Mirror RPM

Using the fastest possible gross laser pulse rate of 200 KHz, it is clear from Figure 21 that a IFOV of 2 mrads leads to an angular velocity of 3,800 rpm. On this basis, there is no need to adopt a complicated dual mirror configuration.

11.3.4 Integral Computing

Based on 50 flops per pixel, Tornado requires 7.5 Mflops to convert coordinates of range pixels. An integral DSP will be provided to perform this transform in real time.

11.3.5 Line Interface

Tornado will provide both line and image interfaces, and will include the ability to access range pixels without transformation in order to support diverse research projects.

11.3.6 Command Interface

Tornado will incorporate a high speed command interface which will permit the application to control the sweep in real time.

11.4 Tornado Simulation

The sensor has been simulated with an elevation stabilization loop and a 4 Hz frame rate giving a 4 degree vertical field of view. On this basis, an image is 1050 rows by 35 columns. The simulation was conducted at 20 m.p.h. The range image at a particular point in the run and the corresponding map are given below:

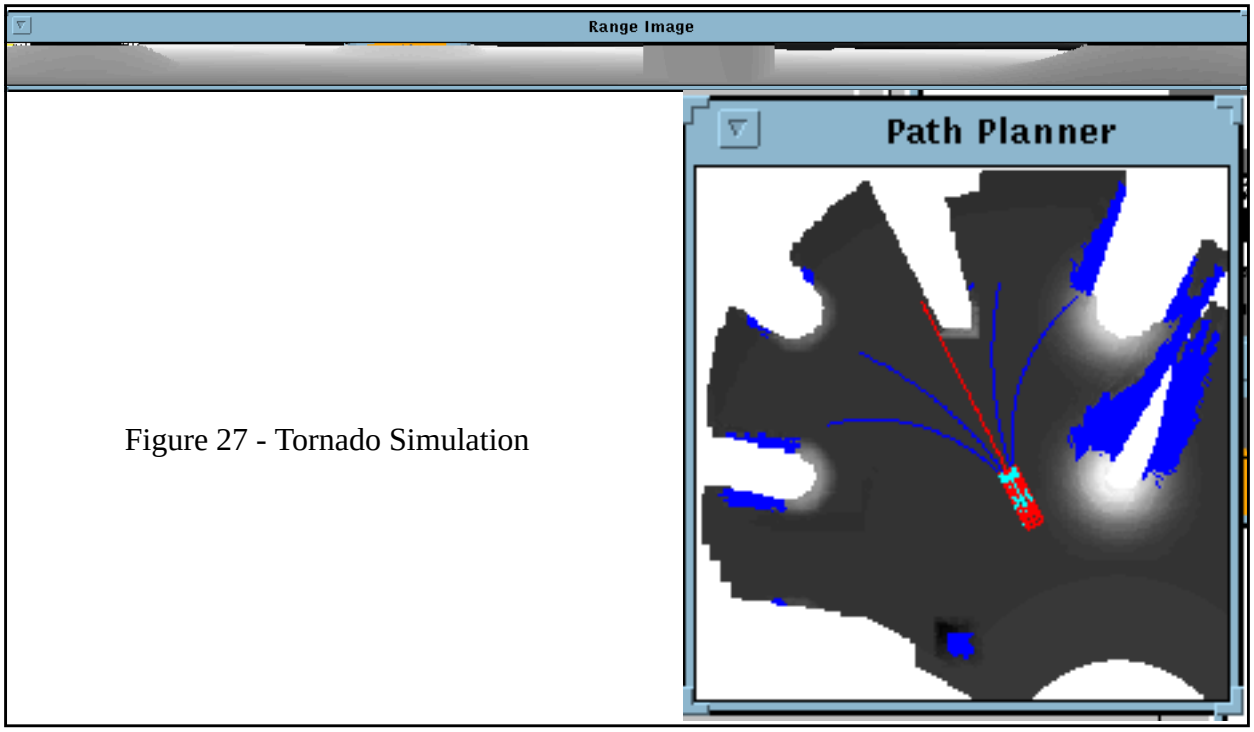

Figure 27 - Tornado Simulation

The relative size of the vehicle and the map tells the whole story. Compared to the ERIM, this sensor has five times the resolution, five times the throughput, twice the frame rate, and almost twice the horizontal field of view. While vertical field of view has been sacrificed, the mechanism of pointing the sensor farther downrange makes this irrelevant and also enhances obstacle detectability.

There is some value in investigating the ramifications of trying to get the laser vendor to reduce the beam dispersion below 2 mrads.

11.5 Summary

This section has established the following:

- A practical laser rangefinder can be constructed today which is custom engineered for high speed autonomous vehicles. Such a system will make 20 m.p.h. speeds possible.
- This is possible through the specification of a system which is designed specifically for the high speed navigation problem.
- Tornado is a rangefinder which, in one package, addresses all of the strategic goals set out in [5]. It is a real time system which is adaptive, high resolution, long range, with integral high performance computing and position estimation.

12. Scanner Comparisons

12.1 Scanner Comparisons

The Tornado is designed specifically to support high speed motion. The specifications for some well known scanners and the Tornado are summarized in the following tables:

Table 4: High Sweep Rate Scanner Specifications

Spec.	ERIM	Perceptron
HFOV	80 degrees	60 degrees
VFOV	30 degrees	90 degrees programmable
IFOV	10 mrad	5 mrad
Frame Rate	2 Hz	2 Hz programmable
Vertical Sweep Rate	75 degrees/sec	170 degrees/sec
Scan Type	Azimuth	Azimuth
Net Bandwidth	32 KHz	130 KHz

There are two scanners which may be considered low speed scanners. These scanners opt for higher angular resolution and sacrifice speed.

Table 5: Low Sweep Rate Scanner Specifications

Table 6:

Spec.	Hurricane	Odetics (proposed)	Tornado
HFOV	360 degrees	50 degrees	120 degrees
VFOV	40 degrees	30 degrees programmable	60 degrees programmable
IFOV	3 mrad	1 mrad	2mrad
Frame Rate	2 Hz	2.2 Hz programmable	4 Hz programmable
Vertical Sweep Rate	3 degrees/sec	34 degrees/sec	16 degrees/sec
Scan Type	Elevation	Unknown	Elevation
Net Bandwidth	20 KHz	500 KHz (proposed)	150 KHz

13. Further Work

13.1 Active Dispersion Control - Size

One of the most important factors in determining the geometric efficiency of a rangefinder is the uniformity of the scan measured in the groundplane. Even though conventional lasers pulse at high rates, up to 90% of the information they provide is redundant. A uniform cartesian scan has been proposed here because active collimation is hard to achieve with off the shelf components.

If such technology could be purchased or developed, an order of magnitude increase in performance will be available. It has already been argued that such an increase is necessary in order to completely meet the system requirements.

13.2 Pixel Aspect Ratio

The pixel aspect ratio on the ground varies from 16:1 to 8:1. Hence, if the beam was deformed to say 1:12 on input, the overall shape of pixels would better approximate a circle on average. Even more important, an order of magnitude increase in frame rate could be achieved at no computational cost ***provided a faster scanning mechanism could be achieved***. Even if the azimuth could not be suitably deformed, spacing pixels in azimuth also increases the frame rate provided fast enough mirrors could be achieved.

13.3 Multifaceted Nodding Mirror

One of the primary requirements which Tornado fails to meet is the ability to detect potholes in sufficient time to react to them. At low speeds, it may be possible to use a multifaceted nodding mirror to quickly place a small number of scanlines near the vehicle without sacrificing throughput. It will be necessary to study the vignetting of the receive beam to ensure that this is possible. At high speeds, this approach may not be feasible at all because the point at which a pothole can be recognized is well inside the stopping distance.

14. Problems of the ERIM Scanner

This report has shown indirectly that many problems exist with the ERIM configuration which effectively limit speed to about 3 m/s and simultaneously make it unreliable even at that speed. As a motivation for the Tornado scanner, consider the following rough calculations of the limits placed upon the speed of the HMMWV by the ERIM scanner.

14.1 Angular Resolution and Maximum Range

Two independent experiments have concluded that the ERIM scanner cannot resolve a wheel collision hazard before it reaches ten meters range. It is clear from Figure 2 that this corresponds to a vertical spot size of 0.1 meters at the ERIM beam dispersion of 10 mrads. So this is predicted by the analysis here. On this basis, the effective maximum range of the sensor is only ten meters. Many results of [5] indicate that even perfect obstacle detection at that range is consistent with at most 3 meter/second speeds. These conclusions are consistent with the actual performance of the vehicle in experiments.

14.2 Impulse Turning to Avoid a Wide Step

If only 10 meters remain before a wide step obstacle is detected, and it takes 7.5 meters to execute a turn, the vehicle must detect the obstacle and turn the steering wheel to full deflection before moving 2.5 meters if it is to avoid a wide step obstacle. If this is to be achieved at even 3 m/s speed, the system reaction time must be less than a second. The current reaction time for steering cannot possibly be less than 2 seconds, and it is likely 3 seconds, so the HMMWV cannot possibly avoid such obstacles reliably at even 3 m/s.

14.3 Slight Turn to Avoid Small Step

If a slight turn is used to avoid a small step obstacle, the finite width of the vehicle is a major factor which reduces the effective range available for obstacle detection. Let 3 meters be allocated for the vehicle to cross its own initial trajectory centreline. This leaves 7 meters to do everything else. If software cycles at 1 second, it contributes 2 seconds to the reaction time, and the steering wheel requires, say, 1/2 more second to respond in a slight turn. Assuming perfect obstacle detection at 10 meters range, maximum speed is limited to 3 meters/second.

14.4 Impulse Turning to Avoid A Large Obstacle

Turning is the preferred mode of obstacle avoidance. Yet, if it takes 7.5 meters to turn 90 degrees, only 12.5 meters remain to allow the vehicle to detect and react to a large obstacle. A large obstacle will require several meters depth in an image in order to know that it is large, so, really only about 10 meters of useful range are available. System reaction time for a 90 degree turn is about 4 seconds assuming software cycle times on the order of one second. This means that speed is limited to 2.5 m/s for this maneuver. This is consistent with the need to slow significantly before such obstacles are encountered in experiments. Often, the system fails to turn fast enough for wide obstacles.

15. Bibliography

[1] O. Amidi, “Integrated Mobile Robot Control”, Robotics Institute Technical Report CMU-RI-TR-90-17, Kelly, A., “A 3D State Space Formulation of a Navigation Kalman Filter for Autonomous Vehicles”, CMU-RI-TR-XXX

[2] J. Gowdy, A. Stentz, and M. Hebert, “Hierarchical Terrain Representation for Off-Road Navigation”, In Proc SPIE Mobile Robots 1990.

[3] A. J. Kelly, “Essential Kinematics for Autonomous Vehicles”, CMU Robotics Institute Technical Report CMU-RI-TR-94-14.

[4] A. J. Kelly, “Modern Inertial and Satellite Navigation Systems”, CMU Robotics Institute Technical Report CMU-RI-TR-94-15.

[5] A. J. Kelly, “A Partial Analysis of the High Speed Autonomous Navigation Problem”, CMU Robotics Institute Technical Report CMU-RI-TR-94-16.

[6] A. J. Kelly, “A Feedforward Control Approach to the Local Navigation Problem for Autonomous Vehicles”, CMU Robotics Institute Technical Report CMU-RI-TR-94-17.

[7] A. J. Kelly, “Adaptive Perception for Autonomous Vehicles”, CMU Robotics Institute Technical Report CMU-RI-TR-94-18.

[8] A. J. Kelly, “A 3D State Space Formulation of a Navigation Kalman Filter for Autonomous Vehicles”, CMU Robotics Institute Technical Report CMU-RI-TR-94-19.

[9] A. J. Kelly, “An Intelligent Predictive Controller for Autonomous Vehicles”, CMU Robotics Institute Technical Report CMU-RI-TR-94-20.

[10] M. Hebert and E. Krotkov, “Imaging Laser Radars: How Good Are They”, IROS 91, November 91.

[11] M. Hebert. “Building and Navigating Maps of Road Scenes Using an Active Sensor”, In Proceedings IEEE conference on Robotics & Automation, 1989; pp.36-1142.

[12] M. Hebert, T. Kanade, and I. Kweon. “3-D Vision Techniques for Autonomous Vehicles”, Technical Report CMU-RI-TR-88-12, The Robotics Institute, Carnegie Mellon University, 1988

[13] B.K Horn and J. G. Harris, “Rigid Body Motion from Range Image Sequences”, Image Understanding, Vol 53, No 1, January 1991, pp 1-13

[14] Hoffman, R., Krotkov, E., “Terrain Mapping for Outdoor Robots: Robust Perception for Walking in the Grass”, Submitted to IEEE International Conference on Robotics and Automation, 1993.

[15] In So Kweon, “Modelling Rugged Terrain by Mobile Robots with Multiple Sensors”, CMU PhD Thesis, 1990

Index

S

U

V